Geochimica et Cosmochimica Acta 391 (2025) 1–15

Contents lists available at ScienceDirect

Geochimica et Cosmochimica Acta

journal homepage: www.elsevier.com/locate/gca

Processes controlling nickel and its isotopes in anoxic sediments of a seasonally hypoxic bay

Sarah Fleischmann [a,*], Florian Scholz [b], Jianghui Du [a,c], Jan Scholten [d], Derek Vance [a]

[a] Institute of Geochemistry and Petrology, Department of Earth and Planetary Sciences, ETH Zürich, Clausiusstrasse 25, 8092 Zürich, Switzerland
[b] Institute for Geology, Center for Earth System Research and Sustainability, Universität Hamburg, Bundesstraße 55, 20146 Hamburg, Germany
[c] Key Laboratory of Orogenic Belt and Crustal Evolution, MOE, School of Earth and Space Science, Peking University, Beijing 100871, China
[d] Department of Geosciences, Kiel University, Otto-Hahn-Platz 1, 24118 Kiel, Germany

ARTICLE INFO

Associate editor: Natascha Riedinger

Keywords:
Nickel
Ni isotopes
Organic-rich sediments
Porewaters
Oceanic mass balance

ABSTRACT

Nickel (Ni) is a biologically active metal whose reactivity and isotope fractionation in the marine realm are strongly influenced by biological and redox-related processes, giving the stable isotope system potential for studying past ocean environments. Reducing, organic-rich, sediments constitute an important sink of Ni from the modern ocean. Importantly, at open ocean upwelling margins, these kinds of sediment record the isotope composition of the modern deep ocean. Thus, records of their Ni isotope composition in the past have the potential to record the past deep ocean isotope composition and the oceanic isotope mass balance. However, the detailed processes controlling the upwelling sink are not fully understood. Here, we address this issue through data for sediments, porewaters and the water column of Kiel Bight in the Western Baltic Sea. This setting preserves sediments that have similar characteristics to those of open ocean upwelling margins, allowing us to study specific controlling processes in a well constrained setting.

In common with sediments from open-ocean upwelling settings, Ni is well-correlated with carbon in solid sediment, suggesting delivery of Ni via rain of organic carbon from the water column. Overall, porewaters at all sites studied show increasing Ni concentrations from around 10 nM near the sediment–water interface to as high as 50 nM at 25 cm depth. This increase is correlated with increases in ammonia concentrations, suggesting release of Ni from anaerobic respiration of organic matter. However, porewater Ni/NH_4 ratios are always lower than Ni:N of water column suspended particulate matter, suggesting an additional process that removes Ni from the porewater. Porewater sulphide also increases with depth, from as low as zero at the sediment–water interface to levels as high as 3 mM at 25 cm. Overall, porewater Ni isotopes become heavier with depth, from bottom water δ^{60}Ni around +0.5 to +1‰, to values as high as +2.3‰ at depth. All these observations strongly suggest that Ni is removed from porewater into a solid sulphide. Mass balance indicates that over 90% of the Ni delivered in organic material to the sediment–water interface is transferred from organic matter into solid sulphide. Upward diffusive fluxes lead to the loss of a small amount back to the water column via a benthic flux. Given the large proportion of Ni retained within the sediment, the loss of such Ni does not strongly impact the isotope composition of the buried pool. These data are crucial in clarifying the processes controlling the size and isotope composition of organic-rich sediments on upwelling margins.

1. Introduction

Nickel (Ni), like many other transition metals, shows a nutrient-like distribution in the oceanic water column (e.g., Sclater et al., 1976; Bruland 1980; Mackey et al., 2002). Low concentrations in the photic zone reflect uptake by phytoplankton to fulfil key roles in a number of enzyme systems (Ragsdale, 2009). The activity of these enzymes in turn plays important roles in a number of global biogeochemical cycles, including those of carbon, nitrogen- and oxygen. Recent advances in the analysis of Ni isotopes (expressed as δ^{60}Ni) have opened new perspectives for the development of Ni as a tracer of the chemistry of past ocean environments. In particular, Ni isotope compositions are significantly fractionated by redox-controlled output fluxes from the oceans to sediments (e.g., Fleischmann et al., 2023) and may be used to track changes

* Corresponding author.
E-mail address: sarah.fleischmann@eaps.ethz.ch (S. Fleischmann).

https://doi.org/10.1016/j.gca.2025.01.016
Received 28 September 2024; Accepted 15 January 2025
Available online 19 January 2025

in the redox conditions of the past ocean (e.g., Wang et al., 2019).

In order to develop this relatively new isotope system into a useful tracer for application to Earth history, a number of recent studies (e.g., Cameron and Vance, 2014; Vance et al., 2016; Ciscato et al., 2018; Little et al., 2020; Gueguen et al., 2021; Gueguen and Rouxel, 2021; Revels et al., 2021; He et al., 2023; Fleischmann et al., 2023; Bian et al., 2024a) have focused on gaining a better understanding of the modern oceanic mass balance of Ni and its isotopes, that is the fluxes of Ni into and out of the ocean. The Ni isotope composition of dissolved Ni in the deep ocean (beneath 500 m) is relatively homogeneous, with an average δ^{60}Ni of 1.33±0.13‰ (2SD, where δ^{60}Ni is given as the per mil deviation of the ^{60}Ni/^{58}Ni ratio from NIST SRM986; data compiled in Lemaitre et al. (2022, recently confirmed by further extensive data for the deep Pacific in Bian et al. (2024b)). The main input of Ni to the ocean is via rivers, for which the global input has been estimated at around 0.8‰ (Cameron and Vance, 2014; Revels et al., 2021). Recently, Bian et al. (2024a) have suggested that there may be a further input of heavy Ni due to a diffusive flux out of sediment, driven by release of Ni from detrital material and subsequent isotope fractionation due to partitioning of light isotopes from porewaters into Mn oxides. The size of such an input is currently unknown but, in the context of our current understanding of oceanic Ni sources and sinks, Bian et al. (2024a) estimate that it may amount to about 18% of the riverine dissolved input.

The ultimate repository of Ni leaving the oceanic dissolved pool is burial in marine sediment. The smallest of the modern sedimentary sinks is found in euxinic marginal basins (e.g., Black Sea), which bury Ni that is isotopically light compared to seawater (δ^{60}Ni = 0.45‰, Vance et al., 2016). The two biggest outputs of Ni from the oceanic dissolved pool are (1) to oxic open-ocean Mn-oxide-rich sediments and (2) to organic-rich sediments, whose porewaters contain sulphide, at upwelling ocean margins. Mn-oxide particulates strongly sorb Ni, removing it from aqueous solution (Goldberg, 1954). The resulting sediments exhibit a very wide range of authigenic Ni isotope compositions (δ^{60}Ni ~ -1.5 to +2.5‰, Gall et al., 2013; Gueguen et al., 2016, 2021; Little et al., 2020; Gueguen and Rouxel, 2021; Fleischmann et al., 2023). Nickel in organic-rich upwelling sediments is strongly associated with organic carbon (Böning et al., 2015), to which it appears to be transported after uptake into cells in the photic zone and within which it is fixed into solid sulphide (Böning et al., 2015; Ciscato et al., 2018; Plass et al., 2021; Gäng et al., 2023). Studies of locations where organic matter dominates sedimentary Ni budgets, such as the Peru and Namibian margins, have documented authigenic Ni isotope compositions that are identical to the deep ocean (Ciscato et al., 2018; He et al., 2023).

Many of these studies have discussed the apparent imbalance between inputs and outputs to the oceanic dissolved pool and its potential resolution. The earliest papers (e.g., Cameron and Vance, 2014) assumed that the size and isotope composition of the important Mn-oxide sink could be obtained from the Ni/Mn ratio and Ni isotope composition of Fe-Mn crusts (Gall et al., 2013; Gueguen et al., 2016; 2021). However, such an approach leads to an output flux that is much greater and isotopically heavier than the known inputs (e.g., Cameron and Vance, 2014). Two potential ways have been suggested that could resolve this mass balance problem. Fleischmann et al. (2023) point to studies that suggest that Fe-Mn crusts represent a tiny proportion of the global Mn output flux (Uramoto et al., 2019), and that a very substantial proportion of the Mn output is to proximal hydrothermal sediments, which scavenge Ni from seawater (e.g., Gueguen et al., 2021). They combine this with new measurements of Ni abundances and isotope compositions in Mn-rich abyssal sediments, as well as a compilation of data for proximal hydrothermal sediments, to suggest that the oceanic Ni elemental and isotope budget is readily balanced if the Mn oxide output represents a mixture of these two types of sediment.

Other studies have raised the possibility that diagenetic reactions in sediment lead to release of isotopically heavy Ni to the pore water followed by diffusion across the sediment–water interface back to the water column (Atkins et al., 2016; Little et al., 2020; Gueguen and Rouxel, 2021; Bian et al., 2024a). However, the size and isotope composition of such putative benthic fluxes are poorly known due to the lack of porewater data for Ni concentrations and isotope compositions. Porewaters from fully oxic open ocean Mn-rich sediments have yet to be measured. Bruggmann et al. (2024) and Bian et al. (2024a) have recently presented data for intermediate settings where Mn oxide is stable at the sediment–water interface but is being reduced deeper within sediment. He et al. (2023) and Bruggmann et al. (2024) have recently presented Ni concentration and isotope data for the organic-rich sediments (with shallow sulphidic porewaters) of the Namibian and California Margins. Though these studies hint at a significant flux back out of such organic-rich sediments, the processes controlling and driving this flux are only partially understood.

Here, we present data for organic-rich sediments from the Baltic Sea (Kiel Bight). Kiel Bight has a broad range of sedimentary redox conditions over a small area, making it an ideal location to investigate the impact of changing redox conditions on the benthic flux of trace metals such as Ni. Our study has two main objectives. First, we add to the extremely scarce data for Ni abundances and isotope compositions in porewaters, from any kind of sediment. Our study site allows us to undertake a more detailed analysis than heretofore of the specific diagenetic processes that control fluxes back across the sediment–water interface in anoxic settings, and that determine their isotope composition. Second, we use the data to assess the degree to which such diagenetic processes modify the isotope composition of the sediment solid phase. Authigenic Ni in bulk organic-rich sediments has an average isotope composition of +1.29±0.12‰ (Ciscato et al., 2018; He et al., 2023), which is similar to the average δ^{60}Ni of seawater. These sediments have potential to be used as an archive to study the Ni isotope composition of the past ocean. It is therefore important to understand the processes operating in this setting, particularly those that may modify the buried Ni isotope composition.

2. Study Site

The Kiel Bight is a shallow marginal area of the Western Baltic Sea and connects the Baltic Proper with the Danish Straits (Fig. 1). The Kiel

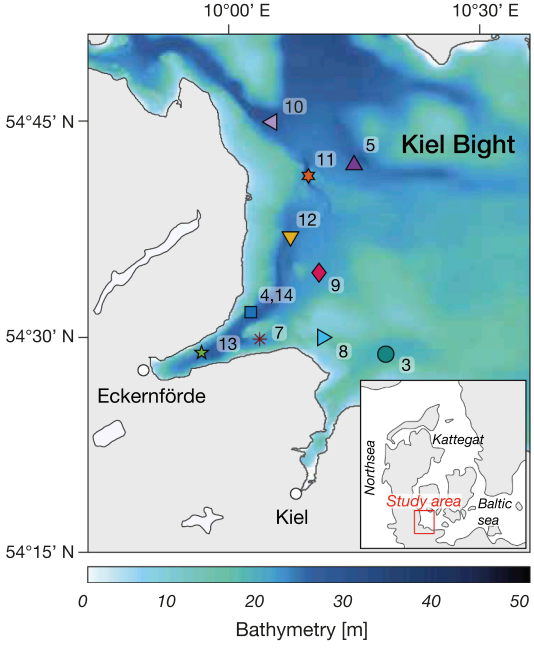

Fig. 1. The Kiel Bight and its position in the Baltic Sea. Coloured symbols indicate the locations of the stations sampled for sediment and porewaters. "Boknis Eck", one of the longest-operated time series stations worldwide, is located at point 4,14.

Bight was shaped by the Scandinavian Ice Sheet, which left a complex system of carved channels and ground moraine ridges (Seibold et al., 1971). At the present day, sediments are largely supplied by coastal erosion and redeposition of material from the sea bottom. Erosion of Pleistocene till in cliffs on the surrounding shore line and at submarine ridges represents the main source of sediments to the Kiel Bight. The glacial till is mainly composed of rock debris containing quartz, feldspar and clay minerals and about 20% of $CaCO_3$ (Seibold et al., 1971). The coarse-grained material is mainly retained in shallow areas whereas the fine-grained sediment fraction is transported further offshore and accumulates as fine mud in deep channels and basins (Seibold et al., 1971).

As anthropogenic activities have strongly influenced geochemical cycles in the Baltic since the beginning of the 20th century, the Baltic has been subject to many monitoring and environmental programs. “Boknis Eck”, one of the longest-operated time series stations worldwide is located within our study area (see Fig. 1, location 4,14) and provides important physical, chemical and biological parameters in Kiel Bight (Lennartz et al., 2014).

As a result of a positive freshwater balance in the catchment area and low water exchange through the narrow Danish straits, the Baltic Sea is generally characterized by brackish water and shows large variations in salinity and temperature (Seibold et al., 1971). Temperature and salinity gradients lead to a strong stratification of Kiel Bight from March until September (e.g., Dargahi et al., 2017). Phytoplankton blooms generally occur in spring and autumn and are dominated by diatoms and dinoflagellates (Graf et al., 1983). A large amount of total bloom production is then deposited on the seafloor as organic matter (Smetacek, 1981) which, due to its microbial remineralisation, can lead to the most reducing conditions – from hypoxic, anoxic (Dale et al., 2013) to sometimes even sulfidic (Lennartz et al., 2014; Plass et al., 2021; Scholz et al., 2023) in the bottom waters during summer and autumn. Upon oxygen depletion in near-bottom water in late summer and fall, denitrification consumes the most reactive particulate organic matter fractions and reaches maximum levels in September (Dale et al., 2013). Stratification ends in late fall due to cooling and wind-induced vertical mixing (Hansen et al., 1999).

3. Materials and Methods

3.1. Sampling

During cruise "AL543" in August 2020, water and sediment samples were collected at 10 different stations in the Kiel Bight, from 18 to 30 m water depth (Fig. 1). At all stations, short sediment cores and the overlying bottom water were collected using a minicorer (MIC). The trace metal-clean Benthic Trace Profiler (BTP) (Plass et al., 2022) was deployed at stations 4 (14), 8 and 12 to sample water at 5 different water depths close to the seafloor (0.6–2.6 m).

Before processing the sediment core, overlying bottom water samples were siphoned off with a tube and reserved for analysis. Sediment cores were subsampled at 1–4 cm intervals, anoxically in a glove bag filled with argon gas. The subsamples were then centrifuged for 15 min at 4000 rpm to extract the porewater. An additional sediment aliquot was taken from a parallel MIC and stored in pre-weighed, air tight plastic cups for the determination of water content and porosity as well as for element analyses. In another argon-filled glove bag, the porewater from the centrifuge vials was poured into a syringe with attached filter (0.2 μm, cellulose acetate, not pre-cleaned) and squeezed into 20 ml Zinsser polyvials to be stored for later analysis. An aliquot of these pore and bottom water samples was analysed for alkalinity and concentrations of dissolved iron, phosphate, silicate, ammonium and hydrogen sulphide in the laboratory of the ship. Subsamples for trace element analysis were acidified to a pH < 2 using distilled concentrated nitric acid (samples analysed approximately 6 months after acidification). The near-bottom seawater from the BTP was in-line filtered and acidified with concentrated nitric acid.

3.2. Analytical methods

3.2.1. Chemical compound and element concentration analyses

Aliquots of bottom water and porewater samples were analysed on board for concentrations of NH_4^+, PO_4^{3-}, SiO_4^{4-}, H_2S, and Fe^{2+} by standard spectrophotometric techniques (Stookey, 1970; Grasshoff et al., 1999). Bottom water and porewater SO_4^{2-} concentrations were analysed by ion chromatography. See https://www.geomar.de/en/mg-analytik for details, including quality control measures.

Trace metal concentrations in porewater, bottom water and BTP water samples were measured on a Thermo Scientific Element XR at ETH Zürich. For the analysis, an aliquot of 50 µl pore/bottom water sample was diluted to 1 ml (20 times dilution) with 2% nitric acid. Element concentrations were determined by comparison with an in-house primary standard, and instrumental drift was corrected using an indium internal standard. Accuracy and reproducibility (8–12%, 95% confidence interval) were monitored by replicate analyses of the reference materials SLRS-6 (river water) and SGR-1 (shale). The concentrations of most elements obtained by HR-ICPMS for the SLRS-6 are consistently 82–93% of the certified values. Nickel concentrations obtained by HR-ICPMS are well-correlated with those obtained by isotope dilution ($r^2 = 0.93$), but are also 17±8% lower. The element concentrations presented here have been adjusted upwards to account for these shifts relative to secondary standards.

Sediment digestion for total element concentration measurements was carried out at the GEOMAR Helmholtz Centre for Ocean Research Kiel, Germany. Approximately 100 mg of ground and freeze-dried sediment was completely dissolved on a hotplate (185 °C, 8 h) in supra pure 40% HF, supra pure 65% HNO_3 and 60% $HClO_4$. Digestion solutions of sediments and suspended particulate matter were then measured by ICP-OES. Method blanks and the reference standards PACS-3 (marine sediment, Canadian Research Council), MESS-3 (Marine Sediment Reference Material, Canadian Research Council) as well as the inhouse standard OMZ-2 were measured to monitor the accuracy of the digestion process. The freeze-dried and ground sediment samples were also analysed for total organic carbon (TOC) using an element analyser (Euro EA, HEKAtech) in Kiel. As the core top sediments in particular contained a large amount of seawater, compound and element concentrations in the solid phase were corrected for the amount of salt that entered the solid phase during freeze drying. The correction factor was determined from the water content in the wet sediment, determined by weighing before and after freeze drying, and the salinity. The correction factors are given in Table S4 together with the salt-corrected compound and element concentrations of the solid phase.

Suspended particulate matter (SPM) on filters was digested following the sampling and sample-handling protocols for GEOTRACES cruises (Cutter et al., 2014). In brief, filters were cut into halves, placed into PTFE vials and the SPM were digested through refluxing of HNO_3 and HF on a hot plate. After repeated evaporation of the solution and re-dissolution with concentrated HNO_3, the residue was re-dissolved in 5M HNO_3 and stored for further analysis.

3.2.2. Ni isotope analyses

The bottom waters and porewaters from core MIC 4–3, MIC 5–3, MIC 9–2, MIC 13–2 and selected sediment samples from core MIC 3–2, MIC 4–3, MIC 5–3, MIC 8–4, MIC 10–2, MIC 13–2 were purified for Ni isotope measurements using ion-exchange in the clean labs of the Institute of Geochemistry and Petrology at ETH Zürich. Only double-distilled acids and reagents and deionized high-purity water (Milli-Q water, resistivity = 18.2 MΩ) were used for metal purification. Before column chromatography, aliquots of the samples were spiked with a ^{61}Ni-^{62}Ni double spike. Porewater and bottom water samples were preconcentrated on a small version of the Nobias column described in Vance et al. (2016) and Archer et al. (2020). Apart from this, the purification of Ni mostly followed the procedure in Sun et al. (2021). Here we highlight only the parts of the procedure that differed from that described in previous

papers from this laboratory. An impure Ni fraction from a large anion column was passed through a small anion column loaded with AGMP-1M resin, but modified from the Sun et al. (2021) procedure to use 0.2M HF to remove Al and Sn. In a final step, major cations were removed using a small Nobias column loaded with the chelating resin Nobias PA-1 as described in Sun et al. (2021), but with the addition of two further elution steps: between the ammonium acetate solution and the final Ni elution step with 1M HCl, the addition of 2M NH_4F followed by Milli-Q water cleans up Al, Ti, and Fe and minimises the organic load. The Ni purification procedures for the digested and spiked sediment samples were similar to those for the pore and bottom water samples, with the exception of the initial preconcentration step.

After column chromatography all purified Ni samples were oxidised with concentrated nitric acid and H_2O_2 and dissolved in 2% HNO_3 for the isotopic measurement. Nickel isotope compositions were measured using a Thermo Scientific Neptune Plus MC-ICP-MS at ETH Zürich. The double spike method as described in Archer et al. (2020) was applied to correct for instrumental mass fractionation. The Ni isotope compositions are given in the standard delta notation relative to the NIST SRM986 standard:

$$\delta^{60}Ni(‰) = \left[\frac{\left(\frac{60Ni}{58Ni}\right)_{Sample}}{\left(\frac{60Ni}{58Ni}\right)_{SRM986}} - 1 \right] \times 1000 \quad (1)$$

The two secondary standards USGS NodA1 and NodP1 have been measured repeatedly in the ETH Zurich labs since 2014, to monitor long-term reproducibility of Ni isotopic analyses in our lab. They have given $\delta^{60}Ni = +1.04 \pm 0.07‰$ (2 sigma, n = 561) and $\delta^{60}Ni = +0.35 \pm 0.08‰$ (2 sigma, n = 742), respectively. For the porewaters and bottom water samples the internal error is plotted in the figures since it is always equal to or greater than the reproducibility. For sediment samples the uncertainty of 0.08‰ is plotted in the figures except for one sample where the internal error was greater, at 0.09‰. Twelve total procedural blanks for the entire chemical separation procedure for porewaters and bottom water contained between 0.1 and 2.2 ng Ni. Since most of the processed porewater samples contained only about 20 ng Ni, a blank correction was applied. For the blank correction, the crustal Ni isotope composition of 0.1‰ was used. The average blank correction to $\delta^{60}Ni$ was 0.05‰, though for three samples it was as high as 0.21–0.22‰. No blank correction was applied to sediment samples, which always had more than 89 ng Ni in the processed samples.

3.2.3. Detrital correction of sediment concentration and isotope compositions

A detrital correction as described in Ciscato et al. (2018) and Fleischmann et al. (2023) was applied to determine the authigenic metal abundances and isotope compositions of the sediments, as follows:

$$[Ni]_{authigenic} = [Ni]_{bulk} - [Al]_{bulk} \, x \, (Ni/Al)_{detrital} \quad (2a)$$

$$\delta^{60}Ni_{authigenic} = \frac{\delta^{60}Ni_{bulk} - f_{detrital}\delta^{60}Ni_{detrital}}{f_{authigenic}} \quad (2b)$$

where $f_{detrital}$ and $f_{authigenic}$ are the fractional amounts of detrital and authigenic Ni in the bulk sample. A detrital Ni/Al ratio of 0.0004, measured in coastal cliffs eroding into Kiel Bight, was used, as well as a detrital Ni isotope composition of 0.12±0.11‰ (Revels et al., 2021).

3.2.4. ^{210}Pb sediment dating

For determination of sedimentation rates (SR; in cm yr^{-1}) and mass accumulation rates (MARs; in g cm^{-2} yr^{-1}) (Appleby and Oldfieldz, 1983), about 5–10 g of dried and ground sediment from Station 8 and 10 were placed and sealed in plastic discs. After an equilibration period of at least three weeks, determinations of ^{210}Pb, ^{137}Cs and ^{226}Ra were performed using two high-purity coaxial germanium detectors (CANBERRA BE3830P). ^{210}Pb was measured via its gamma peak at 46.5 KeV, ^{137}Cs via the gamma peak at 661 KeV, ^{226}Ra via the daughters ^{214}Pb (295 KeV, 352 KeV) and ^{214}Bi (610 KeV). Detector efficiencies were determined using RGU-1, IAEA-375 and IAEA-385 certified reference materials. The evaluation of the gamma spectra, as well as calculations of radionuclide activities and associated uncertainties, were performed using the software package ScienTissiME (https://www.scientissime.net/). Sediment mass accumulation rates were calculated using the method described in Sanchez-Cabeza and Ruiz-Fernández (2012).

3.3. Benthic flux calculation

The benthic flux of Ni across the sediment–water interface was estimated using Fick's first law of diffusion (Li and Gregory, 1974):

$$J_i = -\varphi D_i^{sed} \left(\frac{\partial C_i}{\partial z} \right) \quad (3)$$

where J_i is the flux of an element (i), φ is the porosity of the sediments, D_i^{sed} is the effective diffusion coefficient within the sediments, $\partial C_i/\partial z$ the porewater concentration gradient of element (i). Negative flux values are defined as flux out of the sediment, whereas positive flux values indicate a flux into the sediment. The effective diffusion coefficient is related to the empirically derived diffusion coefficients in seawater D_i^{sw} and the tortuosity θ by the following relationship:

$$D_i^{sed} = \frac{D_i^{sw}}{\theta^2} \quad (4)$$

D_i^{sw} values were adjusted to the local temperature, salinity and pressure using the Stokes-Einstein equation (Li and Gregory, 1974):

$$\frac{D_i^{sw}}{D_i^0} \approx \frac{\mu_0}{\mu_{sw}} \quad (5)$$

where D_i^0 is the ionic diffusion coefficient at in situ temperature, atmospheric pressure and infinite dilution, μ_0 is the viscosity of pure water at in situ temperature and atmospheric pressure and μ_{sw} is the seawater viscosity at in situ temperature, salinity and pressure (Boudreau, 1996). The tortuosity θ was approximated from the porosity φ using the following expression from Boudreau (1996):

$$\theta^2 = 1 - ln(\varphi^2) \quad (6)$$

For the concentration gradient we used the concentration difference between the first porewater sample (at 0–1 cm) and the overlying bottom water. We also performed calculations using the slope values obtained by linear regression through the bottom water and the uppermost porewater samples (down to about 4 cm, depending on where the slope starts to change in the core). Using the latter gave slightly lower benthic flux values, but of the same magnitude.

4. Results

Elemental/species abundance data, Ni isotope compositions, as well as mass accumulation rates are presented in Tables S1 to S5 in the Supplementary Material. Fig. 2 groups the cores into three broad categories according to the porewater chemistries near the sediment–water interface: sulphidic with low Fe concentrations (top panels of Fig. 2), ferruginous, with a peak in dissolved Fe in the top 2 cm (middle panels) and manganous, with a peak in dissolved Mn in the top 2 cm (lower panels).

4.1. Sediment porewaters

The redox chemistry of porewaters (Table S1) is shown for all cores in Fig. 2. At all stations, porewater H_2S increases with depth, reaching

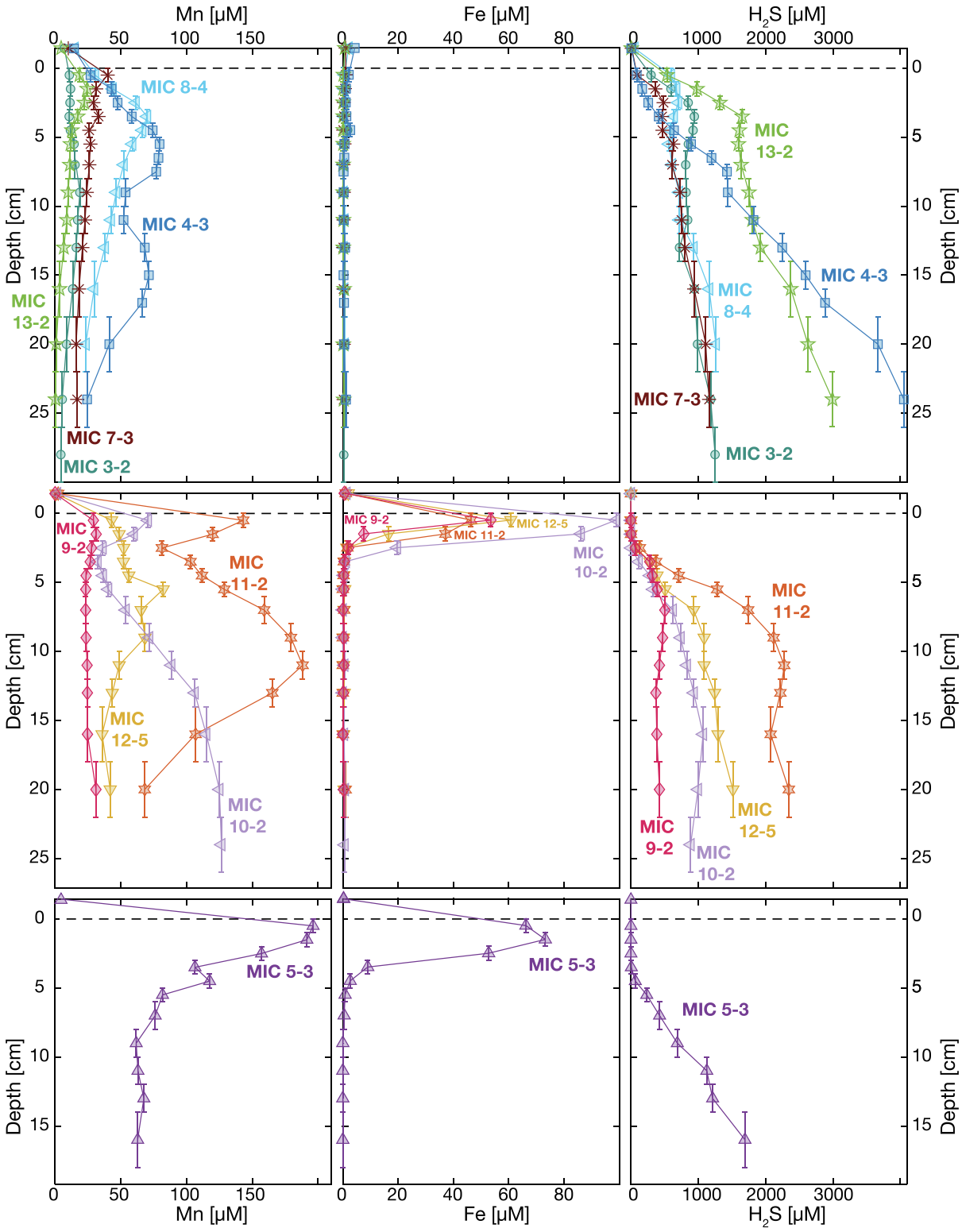

Fig. 2. Dissolved Mn, Fe and H_2S with depth in porewaters of stations 3, 4, 7, 8, 13 (sulfidic at the sediment–water interface), stations 9, 10, 11, 12 (Fe-reducing at the sediment–water interface) and station 5 (Mn-reducing at the sediment–water interface).

maximum values of around 4000 µM in core MIC 4–3. At stations 5 and 9–12, H_2S decreases to zero concentration upwards within the sediment, while at stations 3, 4, 7, 8 and 13 H_2S is detected in bottom water. Total dissolved Fe is very low in the cores that are sulphidic at the sediment–water interface. Sites 5, 9, 10, 11 and 12 show an Fe peak in the top 5 cm, with maximum values of 100 µM (core MIC 10–2). Porewater dissolved Mn shows variable patterns with depth. It is highest in core MIC 5–3, where it increases to a maximum of 200 µM in the uppermost porewater samples and decreases with depth. Nutrients such as, PO_4^{3-}, SiO_4^{4-} and NH_4^+ generally increase in the porewaters with depth at all sites (Table S1). Porewater Ni concentrations range from about 10 nM to maximum values of 60 nM, and generally increase downcore at all the

sites (Fig. 3, Fig. 6, Table S1), indicating a flux of Ni out of the sediment. Porewater Ni isotopes were measured in 4 cores, reflecting different redox environments: MIC 4–3 and MIC 13–2 have sulfidic bottom waters and pore waters. Bottom waters of MIC 9–2 and 5–3 are oxic. The pore water extracted from surface sediments of MIC 9–2 are ferruginous and those from MIC 5–3 are manganous (Fig. 3). Depth profiles of δ^{60}Ni are similar for MIC 4–3 and MIC 5–3, increasing from values of 0.51‰ and 0.87‰ in the bottom waters to maximum values of 1.77‰ and 2.15‰ at a sediment depth of about 15 cm. In MIC 13–2, δ^{60}Ni increases only slightly relative to the bottom water (ca. 0.9‰ difference) in the first 2–3 cm of the core and remains constant at about 1.65‰ downcore. Although δ^{60}Ni in MIC 9–2 also becomes heavier with depth – from 0.7‰ in the bottom water to 2.28‰ at 16 cm – there is more variation in this core, with excursions towards lighter isotope compositions at 2.5 and 9 cm.

4.2. Benthic Trace Profiler water and suspended particulate matter

H_2S concentrations in BTP samples (Table S2) are highest at site 8, where they are constant at around 40–50 µM. Samples from this site also have higher Mn (up to 14 µM) and Fe (up to 2.14 µM) concentrations compared to samples from site 4 (14) and 12. At site 4 (14), H_2S gradually decreases from 3.86 µM at 0.60 m from the bottom to 0 µM at 2.60 m above the seafloor (Fig. 3), whereas at site 12 H_2S-free conditions extend down into the uppermost porewaters. Concentrations of nutrients like phosphate and silica are similar in all samples, at about 3.8 µM and 60 µM, respectively. Dissolved Ni concentrations in BTP samples range from 6.41 to 10.7 nM, and show no variation with depth. Nickel and P concentrations in BTP suspended particulate matter (SPM, Table S3) range from 0.046 to 0.851 nmol/l and from about 70 to 450 nmol/l, respectively. The concentrations of Ni and P in SPM remain fairly constant with depth at site 12, and are somewhat more variable at sites 8 and 14. For the latter, a slight decrease in SPM Ni and P concentrations can be observed with increasing distance from the bottom. A regression of the entire dataset suggests ratios of Ni to P in the SPM of about 1.0±0.1 mmol/mol (Fig. 5).

Ni isotopes were only measured on BTP samples of site 4 (Fig. 3), in order to compare them with porewater Ni isotopes from the same site. Ni isotopes (δ^{60}Ni) in these samples range from 1.11 to 1.21‰ and are heavier than the bottom water just above the sediment at 0.51‰. The uppermost BTP sample (2.6 m above the seawater, 1.21‰) is within error of the average global deep seawater Ni isotope composition (δ^{60}Ni = 1.33±0.13‰, Lemaitre et al., 2022).

4.3. Sediments

Salt-corrected TN, TS and TOC in the solid phase generally decrease sharply at the top at all stations and remain fairly constant with depth (Table S4). At station 4 (14), TN and TOC increase with depth in the upper part of the core, before decreasing at a depth of about 10 cm. Total organic carbon (TOC) contents range from a minimum of about 2 wt% to a maximum of about 9 wt%, and are highest at stations 4 (14) and 13. Salt-corrected bulk Ni concentrations in the solid phase average around 30 ppm and are rather homogeneous with core depth at all sites. The sediments are only slightly enriched in Ni compared to the regional terrigenous background, with enrichment factors of around 1.6 (Table S4).

Nickel isotopes of the selected bulk sediments range from +0.08 to +0.27‰ (Table S4) and are significantly lighter than the Ni isotope composition of seawater, but also isotopically lighter than euxinic sediments. In core 5, no substantial change in Ni isotopes with depth can be observed.

Mass accumulation and sedimentation rates were determined for sites 3, 8, 9, 10 and 12 (Table S5). Sedimentation rates are highest at stations 3 and 10 (up to 0.2 cm yr^{-1}), while the lowest sedimentation rates (as low as 0.07 cm yr^{-1}) were found at stations 9 and 12.

5. Discussion

5.1. The source of Ni to the sediment and porewater-system

In principle, and from previous studies, there are three possible sources of authigenic Ni to the sediment-porewater system. Dissolved Ni could be transported from the water column across the sediment–water interface by diffusion. Since Ni concentrations in porewater are much higher than in the bottom water in all Kiel Bight cores (except for MIC 9–2), a downward diffusive flux of Ni across the sediment–water interface can be excluded at these study sites. From previous studies, two main vectors result in the transport of authigenic Ni to sediment in particulate form: sorption to Mn oxides and in organic matter. In fully oxic open ocean settings, sorption of Ni to Mn oxide particulates results in strong correlations between authigenic Mn and Ni in sediments (Manheim and Lane-Bostwick 1989; Gueguen et al., 2016, 2021; Little et al., 2020; Gueguen and Rouxel, 2021; Fleischmann et al., 2023). Sedimentary Mn concentrations are low in Kiel Bight sediments, such that authigenic Mn concentrations obtained via a conventional detrital correction are often negative (Table S4), precluding this process as significant here.

In modern upwelling settings such as the Peru and Namibia margins where high levels of primary productivity and respiration maintain a perennial oxygen minimum zone (OMZ), Ni uptake by phytoplankton cells in the photic zone and transfer of organic matter to the seafloor has been identified as the main pathway for Ni supply to organic-rich sediments (e.g., Böning et al., 2015, Ciscato et al., 2018; Plass et al., 2021; Gäng et al., 2023). This leads to a strong correlation between Ni and TOC in these sediments (e.g., Böning et al., 2015; Little et al., 2015; Ciscato et al., 2018; Plass et al., 2021; Gäng et al., 2023; He et al., 2023). Nickel and TOC concentrations for organic-rich upwelling sediments beneath perennial OMZ (Peru and Namibia) define an array with a Ni/TOC ~ 7.2×10^{-4} g/g (Fig. 4), equivalent to around 147 µmol/mol. However, as pointed out by Böning et al. (2015) and Gäng et al. (2023), there is significant and systematic structure in this correlation. Specifically, Ni/TOC ratios are close to 9×10^{-4} g/g at depths of 20–30 cm for cores within the OMZ, whereas ratios are as low as 4×10^{-4} g/g in core-tops (Fig. 4). The data for organic-rich sediments from Kiel Bight also show a correlation between bulk Ni and TOC content, equivalent to a Ni/TOC ~ 4.7×10^{-4} g/g (~96 µmol/mol).

A number of the above studies (e.g., Böning et al., 2015; Ciscato et al., 2018; Plass et al., 2021) have discussed the fact that the Ni/TOC ratio implied by the tight Ni-TOC correlation for the Peru and Namibia margins is much higher than would be expected from measurements of Ni/C in phytoplankton cells collected from the photic zone (in upwelling regions, mainly diatoms with a Ni/P up to 1.5 mmol/mol, equivalent, given a classical Redfield C/P ratio of 106, to Ni/C up to ~ 15 µmol/mol, equivalent to about 0.7×10^{-4} g/g, Twining and Baines, 2013). Thus, unmodified export of diatom cells to the sediment can only account for a small fraction of the total Ni content in the sediment. The Ni/TOC of the bulk sediment in Kiel Bight cores is also much higher than that of diatoms, which are also the dominant phytoplankton in Kiel Bight. Thus, the Ni content of phytoplankton cells is generally not sufficient to explain bulk sedimentary Ni/TOC ratios in organic-rich sediments. The previous studies have invoked a number of potential reasons for the higher Ni/TOC of sediments compared to fresh phytoplankton cells (Böning et al., 2015; Ciscato et al., 2018; Plass et al., 2021). The main possibilities that have arisen are: (1) the possible dominance of organisms other than diatoms with much higher Ni/C ratios, such as prokaryotic organisms with Ni/C ratios of up to 50 µmol/mol (Twining et al., 2010); (2) scavenging of surplus Ni onto particulate surfaces; (3) preferential remineralisation of C relative to Ni during transport to the sediment–water interface or within the sediment (Böning et al., 2015; Ciscato et al., 2018; Gäng et al., 2023).

The data presented here for water column SPM are relevant to this question. The concentrations of P and Ni in SPM in bottom-near

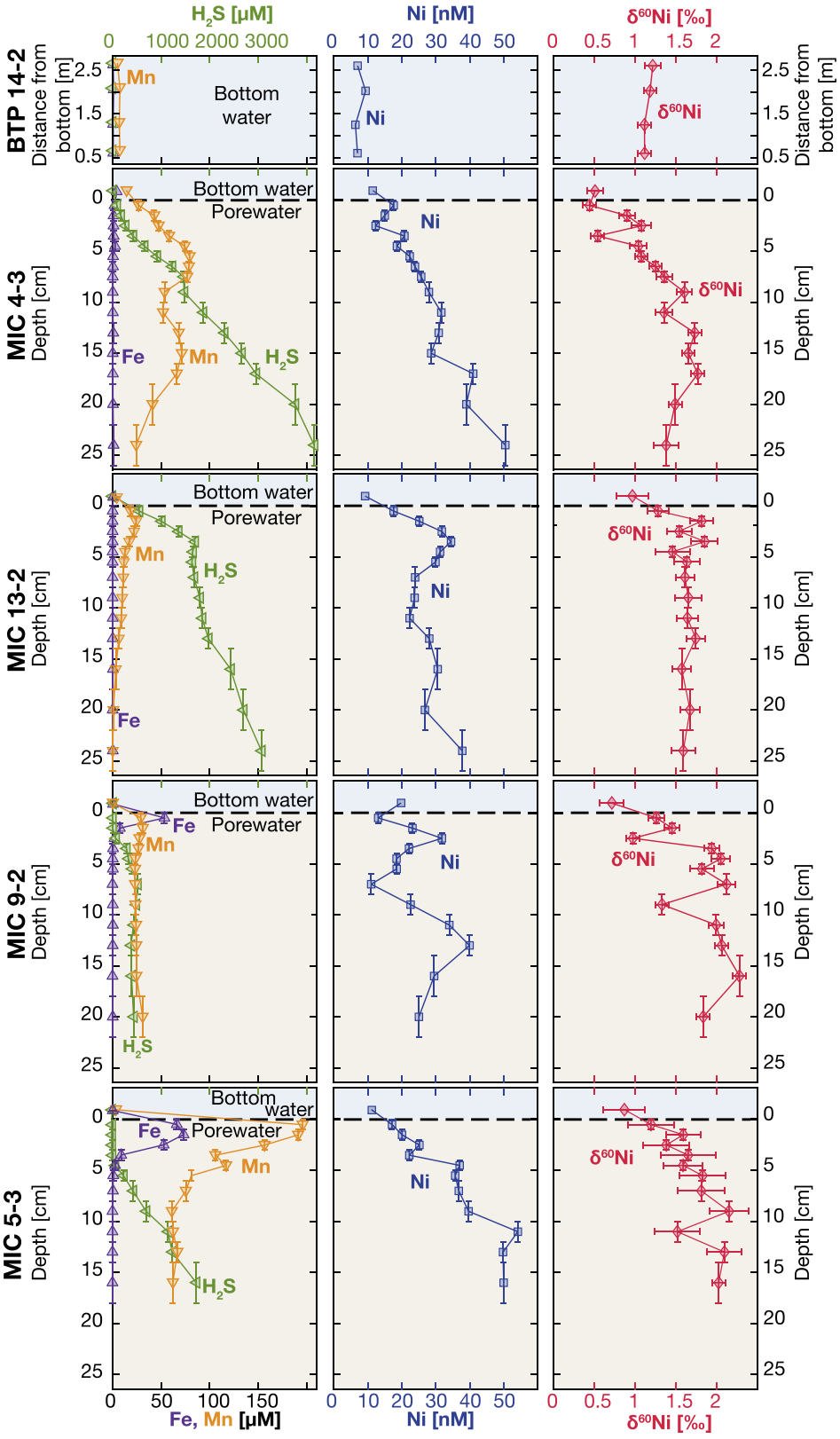

Fig. 3. Dissolved Fe, Mn, H_2S and Ni concentrations and Ni isotopes versus depth in pore water from stations 4, 13, 9 and 5, and in benthic trace profiler samples (bottom water) from station 4. The uppermost point in the depth profiles of the minicore samples corresponds to the overlying bottom water. Nickel concentrations and isotope compositions of the porewaters generally increase with depth beneath the sediment–water interface.

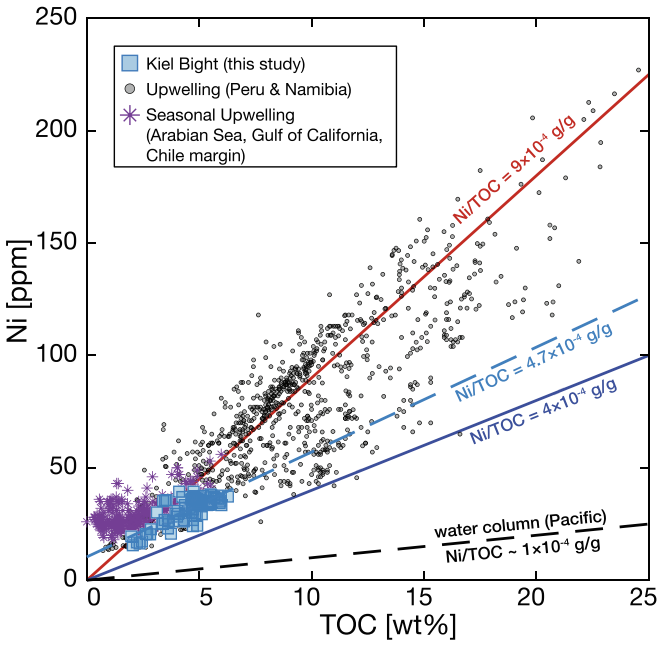

Fig. 4. Bulk Ni [ppm] vs. TOC [%] concentrations for organic-rich sediments from the perennial upwelling settings of Peru and Namibia (Böning et al., 2004, 2015; Little et al., 2015; Ciscato et al., 2018; Plass et al., 2021; Gäng et al., 2023; He et al., 2023) and the seasonal upwelling settings of the Gulf of California, the Arabian Sea and the Chile margin (Brumsack, 1989; Böning et al., 2005, 2009; van der Weijden et al., 2006), compared to data from the Kiel Bight (this study). The red line represents a Ni/TOC ratio of 9×10^{-4} g/g, typical of downcore sediments from Peru and Namibia (Böning et al., 2015; Gäng et al., 2023). For the Peru-Namibia dataset, data that lie below this slope are typically for samples near the sediment–water interface, with Ni/TOC ratios down to around 4×10^{-4} g/g. Ni and TOC concentrations in Kiel Bight sediments also show a linear relationship with a slope of Ni/TOC ~ 4.7×10^{-4} g/g. Note that this figure does not include Kiel Bight sediment samples with high water content (salt correction factor > 1.10), corresponding to the samples of the top 3 cm of most cores, so as to avoid a large error associated with the salt correction.

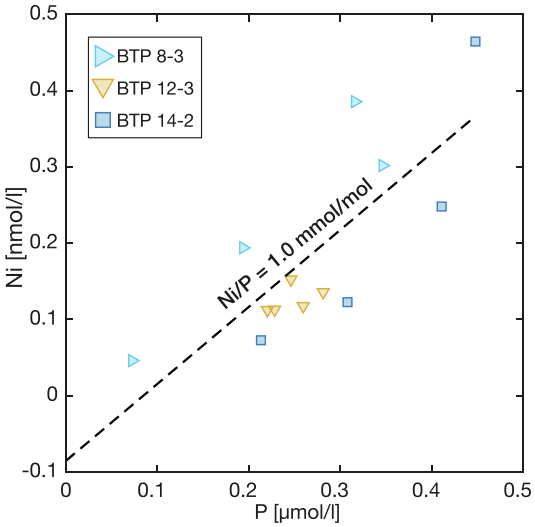

Fig. 5. Ni [nmol/l] vs. P concentrations [µmol/l] in suspended particulate matter of benthic trace profiler samples. Ni is linearly correlated with P in these samples, with a Ni/P of about 1 mmol/mol.

seawater from the BTP in Kiel Bight are also correlated (Fig. 5). Moreover, both the Ni/P implied by this correlation (~1 mmol/mol) and the Ni/C (9.5 µmol/mol) derived from the Ni/P data and a Redfield C/P

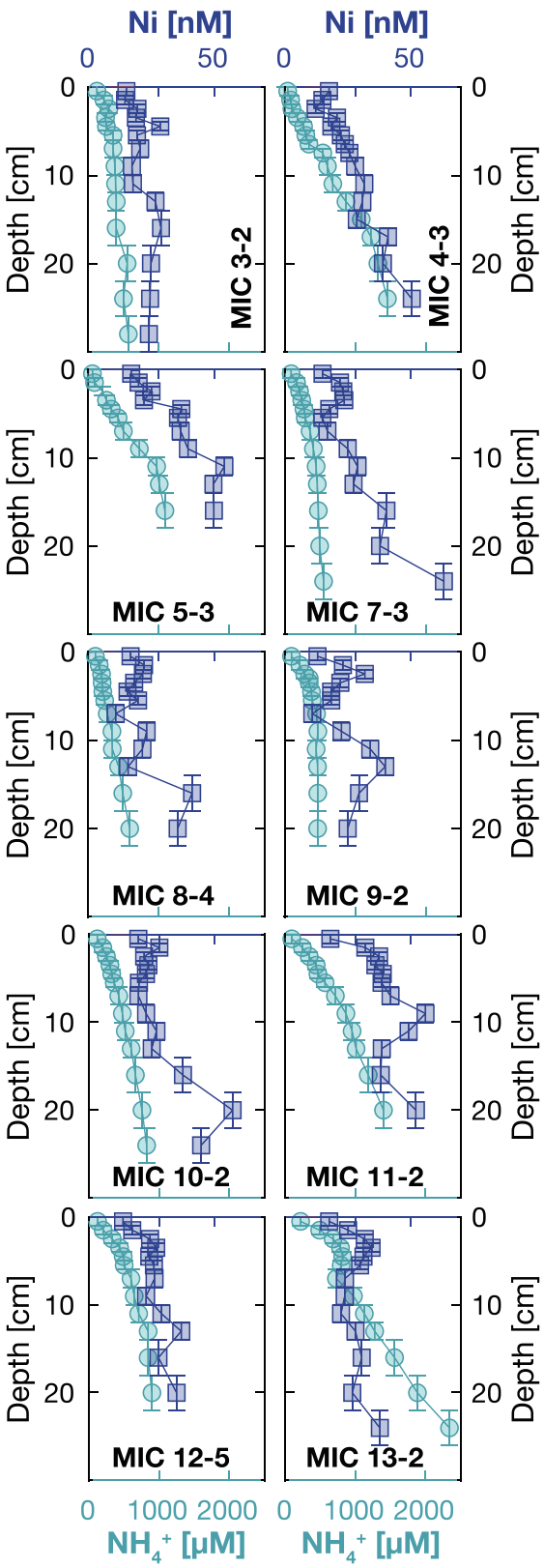

Fig. 6. Porewater depth profiles of Ni (squares) and NH_4^+ (circles) for the investigated cores. The depth profiles of Ni and NH_4^+ concentrations are very similar, with concentrations increasing with depth.

ratio, are consistent with the values reported for diatom cells, and are also much lower than for the sediments. This observation appears to rule out the possibility that scavenging of surplus Ni from the water column explains excess sedimentary Ni over C. Rather, the high Ni/TOC in all these organic-rich sediments is most likely due to preferential remineralisation of carbon relative to Ni, as suggested by previous studies (Böning et al., 2015; Ciscato et al., 2018; Plass et al., 2021; Gäng et al., 2023) and consistent with the fact that Ni/C ratios in Peru and Namibia Margin sediments increase down core. In Kiel Bight cores, the Ni/TOC ratio also increases slightly with sediment depth for most of the cores (Fig. S1), supporting the suggestion that carbon is preferentially lost to the aqueous phase during remineralisation while more of the Ni is retained in the solid phase.

One notable difference between the cores studied here and those from Peru and Namibia is that the δ^{60}Ni of the bulk sediments in Kiel Bight ranges from 0.08 to 0.27‰, much lower than that of local seawater (δ^{60}Ni ~ 1.2‰ in bottom waters from the benthic trace profiler). In contrast, bulk Ni isotope compositions in organic-rich sediments from the Peru and Namibia margins (e.g., Ciscato et al., 2018; He et al., 2023) are close to that of water column dissolved Ni, and authigenic isotope compositions obtained after a correction for detrital material are essentially identical to the deep ocean. However, Kiel Bight sediments are only slightly enriched in authigenic Ni, with Ni/Al ratios that are only around 1.5 times the continental crust (Table S4), mostly around $5–6\times10^{-4}$ (g/g). Ciscato et al. (2018) argued that any detrital correction becomes very uncertain for Ni/Al ratios below about 10×10^{-4} (g/g). Therefore, it is difficult to estimate the isotope composition of authigenic Ni in Kiel Bight sediments in order to make a comparison with the overlying water column, and to use these data as an independent tracer of Ni source. Even ignoring any uncertainty on the detrital Ni/Al ratio, and taking account only of that on the estimate of the detrital Ni isotope composition (Revels et al., 2021), yields a range in estimated authigenic Ni isotope composition of −0.23 to +0.78‰.

In conclusion, our data confirm the strong relationship between Ni and TOC found in other organic-rich sediments (Fig. 4). The authigenic Ni in Kiel Bight sediments mainly originates from organic matter synthesised by diatoms, as indicated by the Ni/C ratios of local water column SPM. The higher Ni/TOC ratio of sediments can be attributed to the preferential remineralisation of carbon relative to Ni within sediment, as has been suggested for sediments from the Peruvian upwelling system (Böning et al., 2015; Ciscato et al., 2018; Plass et al., 2021; Gäng et al., 2023).

5.2. The source of Ni to the porewater

Porewater Ni concentrations in the Kiel Bight pore water generally increase with depth for all cores (Fig. 3). The δ^{60}Ni of the four measured cores also increases with depth, from about 0.5‰ to greater than 2‰, with Ni isotope compositions below and above the δ^{60}Ni of the local deep water (δ^{60}Ni ~ 1.2‰). The upward Ni concentration decrease excludes a diffusive flux of seawater Ni into the sediment. Rather, the Ni in the porewater must originate from particulate carrier phases such as Mn and Fe oxides or organic material. Although some of the porewaters near the sediment–water interface contain small amounts of Fe and Mn (Fig. 2), there is no correlation between porewater Ni and porewater Mn or Fe, arguing against substantial release of Ni to porewaters by dissolution of Mn and Fe oxides.

Similar to Ni concentrations, the major nutrients PO_4^{3-}, NH_4^+ and SiO_4^{4-} in the porewater increase with depth for all cores due to the remineralization of organic matter and opal dissolution. As the concentrations of PO_4^{3-} in our study site are affected by P removal into carbonate fluorapatite (CFA), P release from Fe oxides and preferential P release from organic matter under anoxic conditions (Scholz et al., 2023), NH_4^+ is best suited to trace organic carbon turnover. Unlike Fe and Mn, porewater Ni and NH_4^+ concentrations in the investigated cores increase in a broadly similar way with depth (Fig. 6), hinting that Ni is released into the pore water together with NH_4^+ from organic matter. The relationship between Ni and NH_4^+ in Kiel Bight porewaters is shown in Fig. 7. Starting from the bottom water Ni and NH_4^+ concentrations, indicated by the grey star, the porewater Ni and NH_4^+ values of each core generally increase linearly. The Ni/NH_4^+ ratios are variable, however, with a minimum of around 0.01 nM/μM (MIC 13–2) and a maximum of around 0.04 nM/μM (e.g., MIC 5–3, MIC 10–2). These Ni/NH_4^+ ratios are all lower than the Ni/N of 0.06 nM/μM (red line in Fig. 7) for Kiel Bight water SPM calculated from their Ni/P ratio (~1 mmol/mol, see Fig. 5) and the Redfield N/P ratio. As noted earlier, the Ni/P ratio for Kiel Bight SPM is consistent with values of 0.3–1.5 mmol/mol directly measured in diatoms (Twining and Baines, 2013). Thus, all the data in Figs. 6 and 7 support the suggestion that the dominant source of Ni to porewaters is via remineralisation of particulate organic matter derived from the water column, while the fact that all the porewater data on Fig. 7 lie variably below the Ni/NH_4^+ ratio of water column particulates suggests that there must also be variable loss of Ni relative to N.

The increasing δ^{60}Ni with depth in the porewaters could be the result of either an isotopically heavy source or a light sink. Previous studies have found that authigenic Ni in sediments from upwelling ocean margins, dominated by organic matter, has a similar isotope composition to seawater (δ^{60}Ni of about 1.3‰, Ciscato et al., 2018; He et al., 2023), presumably due to uptake in the photic zone with negligible isotope fractionation. Therefore, organic matter-associated Ni in Kiel bight is expected to have a δ^{60}Ni of around 1.2‰, similar to the uppermost sample of the BTP. In contrast, porewater δ^{60}Ni extend up to 2.3‰. Given that the biogenic source of Ni has been argued above to be the dominant source to porewater, it is most likely that it is a sink of isotopically-light Ni from porewater that controls their observed heavy Ni isotope compositions. One possible sink, that removes isotopically light Ni from the aqueous phase to leave residual heavy isotopes in the porewater, is the removal of Ni to particulate sulphide. In the next section, we test this hypothesis and further explore the controls on δ^{60}Ni in porewater.

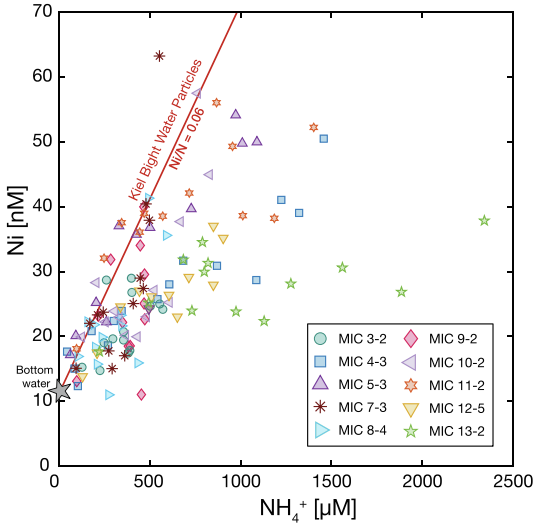

Fig. 7. Porewater Ni (nM) vs. NH_4^+ (μM) concentrations for the investigated cores. Within the same core, the Ni concentration is positively correlated with the NH_4^+ concentration. The grey star indicates the average Ni and NH_4^+ concentration of the bottom waters. The red line represents the Ni/NH_4^+ ratio of 0.06 of Kiel Bight suspended particulate matter, calculated from their Ni/P (see slope in Fig. 5) and the Redfield ratio. The majority of porewater samples plot below the red line and have a Ni/ NH_4^+ < 0.06, indicating a loss of Ni relative to NH_4^+ in the porewaters.

5.3. The sink of Ni from the porewater

The hypothesis that Ni loss from porewaters in Kiel Bight is mainly due to removal of Ni into a solid sulphide phase is supported by other features of the elemental and Ni isotope dataset. Firstly, though solid phase authigenic Ni concentrations are lower than upwelling margins (so that a substantial detrital correction does not permit a precise estimate of an authigenic Ni isotope composition, as noted in section 5.1), they are substantial and positively correlated with authigenic Fe (see Fig. 8A), while in porewaters Fe decreases with depth at most of the sites while H_2S increases (Fig. 2). This is indicative of the formation of a solid phase Fe-sulphide with depth. This observation was also made by Bruggmann et al. (2024) at an upwelling site in Mexico (Soledad), where sediments and porewaters have similar geochemical characteristics to our study site. Secondly, sites with the greatest Ni loss (as indicated by deviations of the Ni/NH_4^+ ratio from that for water column particulates, Fig. 7), such as MIC 4–3 and MIC 13–2, have the highest sulphide concentrations in porewater (Fig. 8B). Fig. 8B also suggests that Ni removal only starts at an H_2S concentration of ~ 200 μM.

The Ni isotope fractionation associated with formation of aqueous Ni sulphide species has been found to be +0.66‰ at 25 °C ($\Delta^{60}Ni_{Ni^{2+}-Ni(HS)^+} = +0.66$‰, Fujii et al., 2014) on the basis of *ab initio* calculations. Natural data from the sulfidic deep Black Sea (Vance et al., 2016) and Namibian margin porewaters (He et al., 2023) show relationships between Ni abundance and isotope composition that are consistent with this fractionation. In the Black Sea, the slight drawdown of Ni from the deep sulfidic water column (beneath 300 m depth), together with an increase in $\delta^{60}Ni$, has been explained by a Rayleigh fractionation model involving transformation of Ni into an aqueous sulphide, with the established theoretical fractionation factor, followed by the instantaneous and quantitative removal of the sulphide species from solution into a solid. Though the nature of the solid is unknown, and though the nature of the removal process (scavenging, saturation of a mineral) is unspecified, the data do not require any further fractionation upon removal. He et al. (2023) document a similar process in porewaters of the Namibian margin.

Fig. 9 explores this process for the Kiel Bight cores for which Ni isotope data are available from this study. In this figure, the Ni/NH_4^+ ratio is used instead of raw Ni concentration to monitor removal, in order to normalise out the impact of additions of Ni to porewater from the biogenic source, and so that the net sink is indicated by a decrease in the Ni/NH_4^+ ratio. The orange arrows in Fig. 9 show the predicted trajectory the data should take, away from a starting porewater pool, under a pure Rayleigh model. Though the Rayleigh model is simple and involves rather extreme assumptions (see below), nearly all the data for cores 4–3 and 5–3 are remarkably consistent with it.

On the other hand, the simple Rayleigh approach does not describe the data trajectories nearly as well for cores 9–2 and 13–2. In the extreme Rayleigh model, the sediment-porewater system as well as each layer within it must act as closed systems. While the overall trend of the data for MIC 9–2 shows a trend that approximates to the orange arrow in Fig. 9, there is a lot of scatter away from it. But the porewater Ni concentration and isotope data for core 9–2 clearly do not conform to an expected steady-state profile. Features such as the reversals in both Ni concentrations and Ni isotope compositions between 3 and 12 cm are almost certainly caused by processes that have disturbed this profile away from a steady-state. Physical disturbances such as transient mixing or irrigation and seasonal changes in organic matter delivery, all processes that are well-known to occur in shallow sediments of Kiel Bight (Dale et al., 2013; Perner et al., 2022), lead to complex patterns in sediment-porewater systems (e.g., He et al., 2021), and clearly violate the closed system assumption.

Core 13–2 shows a very rapid increase in H_2S, to very high levels, down to about 3–4 cm, beneath which the increase is much slower with depth. The same rapid increase is seen in porewater Ni concentrations in the top 3–4 cm, beneath which concentrations show little change. We speculate that these patterns may be responding to the fact that the sequestration of the aqueous sulphide species, once it forms, to a solid is not instantaneous and quantitative. In reality, scavenging of such a species would be likely to follow a rate law and depend on the aqueous concentration of the species itself, as has been modelled for Mo (e.g., Helz et al., 2004; Dahl et al., 2010). Thus, it is possible that the rapid, possibly transient, increase in H_2S near the top of MIC 13–2 leads to the buildup of a relatively large pool of the aqueous Ni sulphide species that is scavenged quickly, leading to the heavy Ni isotopes at around 3–4 cm. It is also possible that this converts nearly all the available Ni at this depth to an aqueous sulphide species. Beneath 3–4 cm, the rather constant porewater patterns may represent a pseudo-steady-state, where the concentration of sulphidised Ni is kept low, close to the slower rate of supply from organic matter, and scavenging removal slows. In this case, Ni concentrations and isotope compositions could remain constant down core while the significant contribution of the lighter sulphidised Ni to

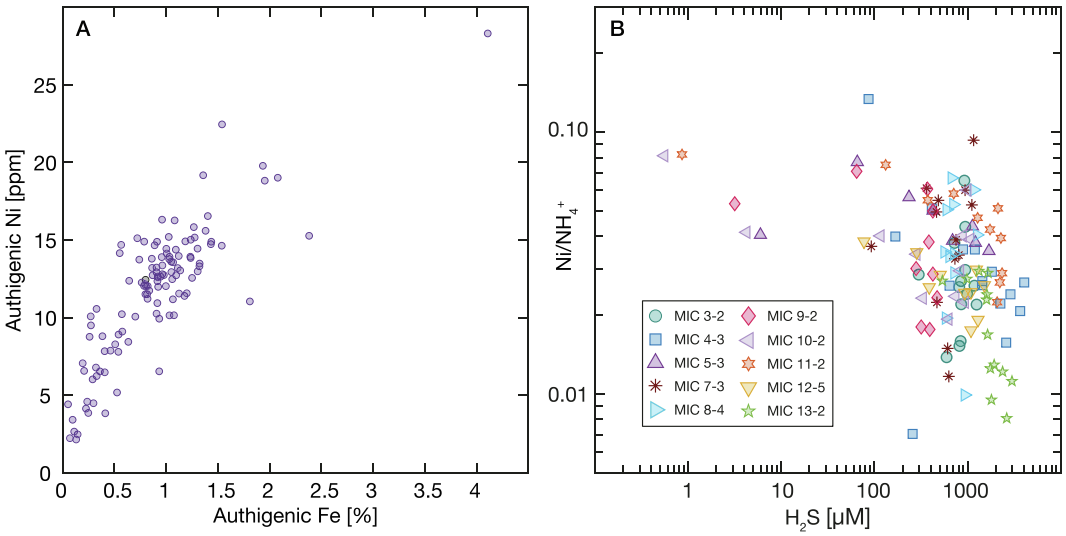

Fig. 8. (A) Crossplot showing that authigenic Ni is positively correlated with authigenic Fe in the solid phase. Authigenic Fe is calculated in the same way as authigenic Ni, but it should be borne in mind that some of this pool may represent detrital Fe oxides that have been converted to pyrite. (B) Porewater Ni/NH_4^+ vs. H_2S [μM] concentrations. Nickel removal relative to NH_4^+ only starts at an H_2S concentration of around 200 μM and the removal rate is highest at site 13. Ni/NH_4^+ ratios in this and Fig. 9 are calculated using Ni concentrations corrected for the bottom water intercept in Fig. 7, i.e., $Ni/NH^+_{sample} = (Ni_{sample} - Ni_{BW})/NH^+_{sample}$.

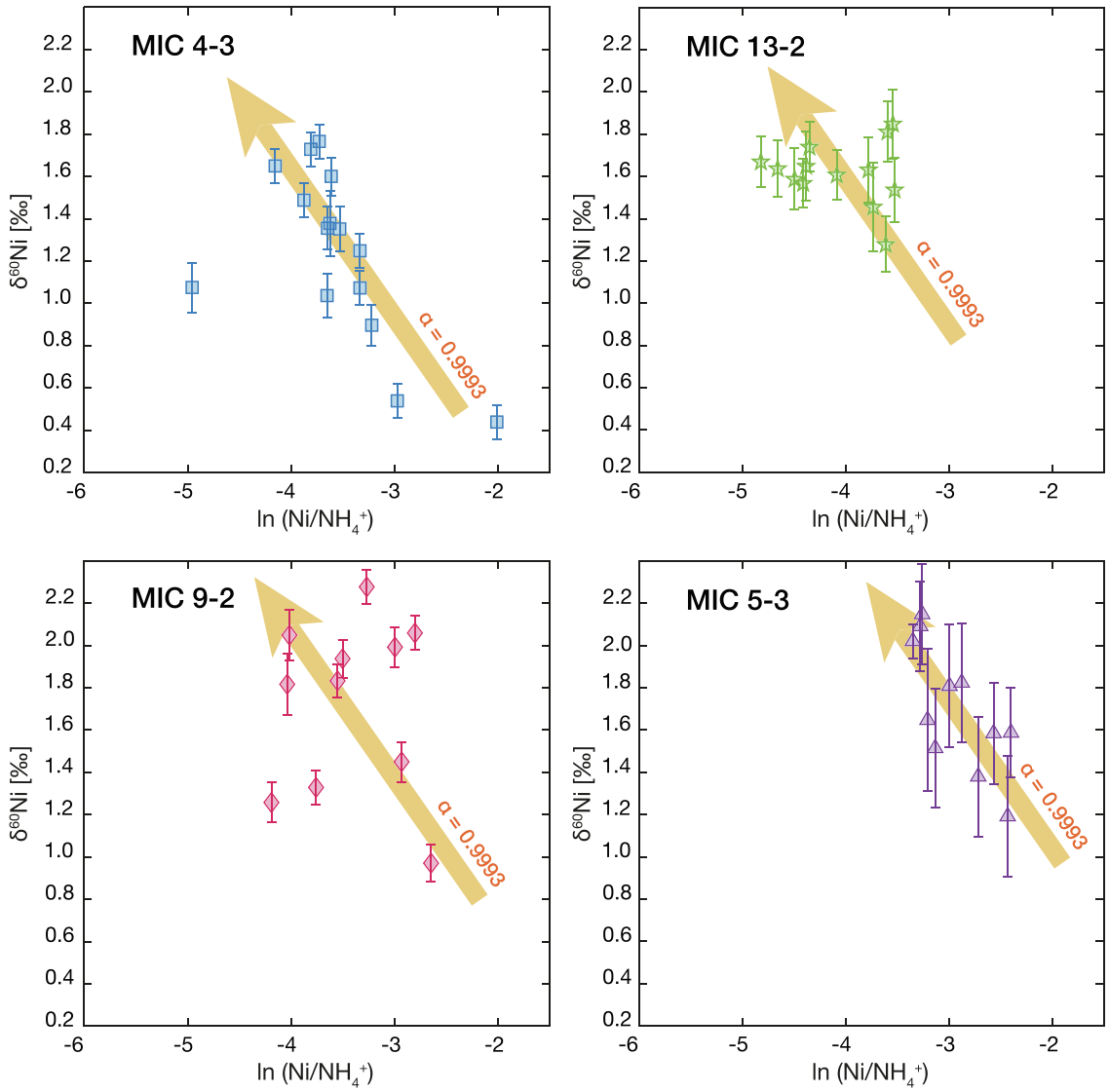

Fig. 9. δ^{60} Ni vs. ln (Ni/NH_4^+) for porewaters of cores MIC 4–3, MIC 13–2, MIC 9–2, and MIC 5–3. The orange arrows show porewater evolution in a pure Rayleigh scenario, whereby Ni is converted to an aqueous sulphide species, with an isotope fractionation factor $\alpha = 0.9993$, and this species is removed instantaneously and quantitatively from solution to a solid. The orange arrow is calculated using the usual Rayleigh formula: $\delta^{60}\mathbf{Ni} = \delta^{60}\mathbf{Ni_{starting}} * \mathbf{f}^{\alpha-1}$, where the δ^{60} Ni in the porewater at the top of the core is the starting point for the model and f is the Ni/NH_4^+ normalized to the value for this starting point.

the aqueous pool would lead to deviations from a pure Rayleigh model (Fig. 9).

A final striking feature of our investigated sites that is not explained by any of the above is that the bottom water at sites 4 and 9 is isotopically lighter (0.51‰ and 0.70‰) than the local seawater Ni isotope composition (~1.2‰). This difference between isotopically light bottom water and heavier seawater is particularly evident at site 4 (Fig. 3). In principle, it is possible that these lighter values are caused by a contribution from the dissolution of detrital material, but we have no robust evidence for such a process. We also note that the conclusion in the recent Bian et al. (2024a) paper that light Ni isotope ratios in porewaters mark a detrital contribution is based on an erroneous suggestion that Mn oxide-associated Ni is never as light as detrital Ni. In fact, Mn-oxide-associated Ni ranges between −1.5 and +2‰ in δ^{60}Ni, encompassing lithogenic values of around 0‰ (Fleischmann et al., 2023). A more likely explanation for the light values in the porewaters of these two Kiel Bight cores is that a small amount of the Ni in the bottom waters is derived from the dissolution of Mn oxides in the uppermost sediment layer. According to natural and experimental data (Vance et al., 2016; Sorensen et al., 2020), Ni adsorbed to Mn oxides can be 3–4‰ lighter than the aqueous phase from which it originates. Thus, if the Mn oxides are derived from local deep water, the Mn-associated Ni in Kiel Bight could have a δ^{60}Ni of −1.8 to −2.8‰ and potentially reduce the overall Ni isotope composition of bottom waters relative to seawater. At site 4, Mn oxide dissolution is expected to be near quantitative and releasing very light Ni to porewaters, whereas at site 9, where the uppermost sediment layer still contains significant amounts of Mn (1266 ppm at the top vs. ~ 300 ppm at the bottom of the core, Table S4), non-quantitative dissolution of Mn oxides might drive the δ^{60}Ni to slightly heavier values compared to the more reducing site 4. Although the δ^{60}Ni of the bottom water in MIC 5–3 (0.87±0.25‰) is within error of the δ^{60}Ni of local seawater (1.21±0.09‰), it is very likely that some of the Ni there also comes from Mn oxides. The contribution of Ni derived from Mn oxides could explain the different Ni/NH_4^+ of different sites (Fig. 7), e.g., why, although sulfidization removes Ni at all the investigated sites, cores MIC 5–3 and MIC 9–2 have high Ni/NH_4^+ compared to more reducing sites such as MIC 13–2, where no Ni is expected to come from Mn oxides.

5.4. The benthic flux of Ni from organic-rich sediments and implications for the global Ni mass balance

In the organic-carbon-rich sediments of the Kiel Bight, diagenetic processes partition authigenic sedimentary Ni, dominantly transferred to the sediment–water interface in particulate organic matter, into three pools: residual, un-respired organic matter, diagenetic sulphide, and the aqueous porewater reservoir. For the latter, the porewater concentration decrease towards the sediment–water interface (Fig. 3) will lead to diffusive transfer of Ni back to the water column, a benthic flux. The first two pools are retained in solid sediment and constitute a net sink for Ni from the water column. The correlation between nickel and carbon in Kiel Bight sediments (Fig. 4) suggests that essentially all authigenic Ni is delivered with carbon at a roughly constant Ni/C ratio, but the Ni/C ratio is a factor of around 10 higher than the particles delivered to the sediment–water interface (section 5.1). Thus, the dominant process retaining Ni in the sediment must be uptake of Ni, re-mobilized into the aqueous phase from organic matter by respiration, into solid sulphide, while the respired carbon is lost back to the water column. This same set of processes operate in the organic-rich sediments of upwelling margins of the modern open ocean (Böning et al., 2004, 2005, 2009, 2015; Ciscato et al., 2018; Plass et al., 2021; Gäng et al., 2023; He et al., 2023), and that control an important sink of Ni in the global ocean, one that is of key significance for the isotope budget (Ciscato et al., 2018; Fleischmann et al., 2023). Thus, the insight gained here on the specifics of this set of processes is highly relevant for the relative importance in the open ocean setting of sedimentary retention versus loss via a benthic flux, including its likely impact on the isotope composition of this sink.

At Kiel Bight, diffusive benthic fluxes of Ni (Table 1) are directed out of the sediment (negative values in Table 1) at all stations, except for station 9 where the porewater profile is most likely out of steady-state. These upward fluxes range from 0.22 to 1.52 nmol cm^{-2} yr^{-1} (Table 1) with an average of 1.08 nmol cm^{-2} yr^{-1} (excluding station 9), and are of the same magnitude and direction as those reported for organic matter-rich sediments from the Peru continental margin (Plass et al., 2021). Recent studies of the California and Mexico Margins (Bruggmann et al., 2024; Bian et al., 2024a) investigate more varied and complex settings, including settings where both organic matter and Mn oxide transfer Ni to the sediment, and where porewater sulphide is variably present. The one site in these latter studies from a setting similar to Kiel Bight and the Peru-Namibia Margin studies cited above is Soledad in Bruggmann et al. (2024). Here, as in the Kiel Bight and on the Peru-Namibia Margins, anoxic bottom and pore waters preclude a significant role for Mn oxide. The main vector for transfer of Ni to the sediment–water interface is organic matter, while reaction with shallow porewater sulphide fixes Ni into the solid phase. The benthic flux out of the sediment at Soledad is of the same magnitude as at Kiel Bight (Bruggmann et al., 2024). Authigenic Ni MARs, where available (station 3, 8, 9, 10, 12), are high compared to these benthic fluxes, implying high Ni burial efficiencies of 83–97% (Table 1, also excluding Station 9), again very similar to the value of 93% reported for the Soledad site (Bruggmann et al., 2024).

In our previous attempts to establish Ni isotope budgets for the global ocean (e.g., Ciscato et al., 2018; Fleischmann et al., 2023), we have quantified the output of Ni to, and burial in, the organic-rich sediments of upwelling margins using the rate of organic carbon burial and the Ni/C ratio of the sediment: in other words, the characteristics of the final buried sediment. This approach yields an estimate for the size of this sink of 1.4×10^{8} mol Ni yr^{-1} (Fleischmann et al., 2023). The clear finding in Gäng et al. (2023) that the Ni/C ratio of these sediments asymptotes to about 9×10^{-4} g/g deep in the sediment suggests the use of this latter as the final buried Ni/C ratio, revising the total Ni sink figure upwards slightly to around 1.54×10^{8} mol Ni yr^{-1}. We also note that a much more recent organic carbon budget (Tegler et al., 2024) suggests burial of about 9 Tg of organic carbon along upwelling margins where bottom-water oxygen decreases below 50 μM, providing another estimate of the Ni burial flux of 1.38×10^{8} mol/yr. In this context, the benthic flux calculated here does not represent a net input to the oceanic Ni budget: the Ni that is lost via the benthic flux is not counted in the previous estimation of the size of the sedimentary sink. It is also important that this Ni sink is relevant only where organic-carbon associated Ni is retained in sediment, which in the Kiel Bight and at open ocean upwelling margins is primarily due to the presence of porewater sulphide at shallow depths. Molybdenum isotope budgets require an areal fraction of this kind of sediment – organic-matter-rich and with sulphide present at shallow depths – of about 1–2% of the global ocean (e.g., Scott et al., 2008; Reinhard et al., 2013; Chen et al., 2015). To the extent that the benthic flux obtained here can be applied to the open ocean settings, it would equate to a global benthic flux of 0.38 (1% of the

Table 1
Benthic fluxes of Ni, authigenic Ni MAR and Ni burial efficiencies.

Sample Sites	Salinity	Temperature (°C)	Water depth (m)	Porosity[a]	D_i^{sed} [b] (10^{-6} cm^{-2} s^{-1})	Benthic flux[c] (nmol cm^{-2} yr^{-1})	δ^{60}Ni benthic flux[d] (‰)	Authigenic Ni MAR[e] (nmol cm^{-2} yr^{-1})	Ni burial efficiency[f]	Fractional flux out relative to input
MIC 3–2	19.65	13.88	18.0	0.777	3.30	−0.60		18.6	0.97	0.03
MIC 4–3	21.00	12.66	28.0	0.804	3.34	−1.05	0.44			
MIC 5–3	20.70	12.06	24.0	0.804	3.29	−1.01	1.19			
MIC 7–3	17.87	15.52	22.0	0.804	3.61	−0.93				
MIC 8–4	19.88	13.53	23.0	0.798	3.39	−1.52		7.62	0.83	0.17
MIC 9–2	19.66	13.88	20.0	0.757	3.19	1.03	1.26	5.00	1.26	−0.26
MIC 10–2	19.81	13.94	26.0	0.834	3.65	−1.49		17.8	0.92	0.08
MIC 11–2	21.07	12.67	29.5	0.804	3.34	−1.40				
MIC 12–5	20.40	12.93	23.6	0.852	3.66	−0.22		7.77	0.97	0.03
MIC 13–2	19.19	14.04	25.7	0.804	3.47	−1.47	1.28			
Average						**−1.08**	**1.04**			

[a] for cores where we didn't have a porosity value, the average porosity of sites 3, 8, 9, 10 and 12 was taken (see Table S5).
[b] see Methods section 3.2.5.
[c] concentration gradient = difference first porewater sample and bottom water sample. Upward fluxes, out of the sediment, are given as negative numbers.
[d] δ^{60}Ni of uppermost porewater sample.
[e] calculated as: average of authigenic Ni conc. of each core × MAR.
[f] calculated as: authigenic Ni MAR/(authigenic Ni MAR-benthic flux), from Berelson et al., 1996.

oceanic area of 3.5×10^8 km^2) – 0.75 (2%) $\times10^8$ mol yr^{-1}. In other words, this tentative global extrapolation would imply total Ni transfer to the sediment–water interface in these settings of 1.76–2.29$\times10^8$ mol yr^{-1}, of which around 70% is buried (1.38–1.54$\times10^8$ mol yr^{-1}).

It is also instructive to compare the above estimates for total Ni delivery to the sediment–water interface with those based on organic carbon rain rates and Ni/C ratios of diatoms. Data for organic carbon rain rates to the sediment–water interface are scarce, including at upwelling zones, but we can undertake a preliminary and illustrative calculation based on data in Dale et al. (2015), who report values of around 10–16 mmol C m^{-2} day^{-1} for two transects across the Peru Margin (averaged across the transect using data in Table 2 and distances taken from Fig. 5 of their paper). The average Ni/C ratio of the dominant phytoplankton transferring carbon and Ni to these sediments – diatoms – is around 1×10^{-5} mol/mol (average of data from Twining et al., 2004, 2011; Twining and Baines, 2013 and discounting one outlier). All this leads to estimates of Ni rain rates for 1% of the oceanic area of 1.3–2.1$\times10^8$ mol yr^{-1}, or for 2% = 2.6–4.1$\times10^8$ mol yr^{-1}. Given that none of these estimates can be very precise, there is some re-assuring self-consistency in the fact that these latter estimates of total Ni delivery rates to the sediment–water interface are close (within a factor of 2 or better) to those obtained by summing estimates of Ni mass accumulation rates and benthic fluxes.

As noted above, the benthic flux back out of the sediments does not impact our previous oceanic Ni budgets (e.g., Fleischmann et al., 2023), because the latter were based on what is observed as buried in the sediment, not on the total delivery of Ni to the sediment–water interface. Moreover, our previous isotope budgets are also based on the characteristics of the net sink as observed in the sediment, with the δ^{60}Ni of authigenic Ni in Peru and Namibia sediments being within uncertainty of the deep ocean value, at +1.29±0.12‰ (Ciscato et al., 2018; He et al., 2023) versus +1.33±0.13‰ (data compiled in Lemaitre et al., 2022). There does exist a possibility of an impact on the preserved isotope composition via the processes described here if, for example, isotope fractionations within the sediment-porewater system lead to a benthic flux that is both a significant fraction of the Ni delivered to the sediment and that is isotopically very different from that Ni. However, the near quantitative retention of Ni in the sediment must mean that any such impact would be very small. In the case of the Kiel Bight the isotope composition of the benthic flux, of the uppermost porewater sample, is similar to the δ^{60}Ni of the local seawater (δ^{60}Ni ~ 1.2‰), except for that at site 4, where the δ^{60}Ni of the surface porewater is lighter (at 0.44‰, Table 1). Even a benthic flux with this latter isotope composition, given Ni preservation rates of around 80–90%, would have minimal impact on the final preserved isotope composition.

6. Summary and concluding remarks

In this contribution, we have investigated the processes that deliver Ni to sediment, as well as those that diagenetically process that Ni, in anoxic, organic-rich sediments. The well-constrained setting of the Kiel Bight, as well as the array of data types presented here, allows us to close mass balances in a way that is rarely possible for open ocean upwelling sites. On the other hand, the controlling processes operating at our study sites are highly relevant to such open ocean upwelling sites, an important sink for Ni in global oceanic terms.

Nickel is delivered to both Kiel Bight and upwelling margin sediments by uptake into phytoplankton cells and rain of organic carbon from the water column to the sediment–water interface, leading to very good correlations between sedimentary Ni and carbon in both types of sediment. In both settings, however, the Ni/C ratio suggested by these correlations is well in excess of phytoplankton ratios, requiring a process that concentrates Ni in the sediment at the expense of carbon. Here, we have shown that porewater Ni concentrations and isotope compositions are controlled by two dominant processes: (1) release of Ni to the aqueous phase via anaerobic respiration of organic matter; (2) removal of Ni, with preferential removal of the light isotope, from porewater into solid sulphide. Mass balance mostly indicates that over 90% of the Ni delivered in organic material to the sediment–water interface is retained in the sediment via these processes. This retention of Ni, in contrast to the loss of respired carbon back to the water column, leads to the order of magnitude higher Ni/C ratio in the sediment relative to the water column particulate source. Upward diffusive fluxes lead to the loss of a small amount of Ni back to the water column. Given the large proportion of Ni retained within the sediment, the loss of such Ni does not impact the isotope composition of the buried pool.

Previous studies (Ciscato et al., 2018; He et al., 2023) have demonstrated that Ni transferred to and preserved in organic-rich sediments at upwelling margins has an isotope composition similar to the deep ocean. The first step in this process, uptake into organic material and delivery to sediment of Ni with deep ocean isotope compositions, presumably reflects minimal isotope fractionations during uptake into cells, combined with the fact that biological uptake removes a large fraction of the upwelled Ni, so that the mass balance means that minimal fractionations are not expressed in any case. The data presented here take our understanding of this sink a step further, by demonstrating that the near-quantitative retention of organic Ni in solid sulphide enhances the preservation of this deep ocean signature, during early diagenetic processes. Our new data do not, however, have implications for our previous estimations of the size and isotope composition of this sink (e.g., Ciscato et al., 2018; Fleischmann et al., 2023), which were based on characterisation of the sediment, the final net sink, itself. Taken together, these studies further highlight the potential of past records of oceanic Ni isotopes of open ocean organic-rich sediments for understanding the past balance of reducing and oxic oceanic sinks, with implications for the evolution of ocean redox through Earth history.

CRediT authorship contribution statement

Sarah Fleischmann: Writing – review & editing, Writing – original draft, Visualization, Validation, Investigation, Formal analysis, Conceptualization. **Florian Scholz:** Writing – review & editing, Validation, Supervision, Resources, Project administration, Investigation, Funding acquisition, Formal analysis, Conceptualization. **Jianghui Du:** Writing – review & editing, Validation, Supervision, Formal analysis, Conceptualization. **Jan Scholten:** Investigation. **Derek Vance:** Writing – review & editing, Writing – original draft, Validation, Supervision, Resources, Project administration, Funding acquisition, Formal analysis, Conceptualization.

Data availability

All the data presented in this manuscript are available through PANGAEA here: Fleischmann, Sarah; Scholz, Florian; Du, Jianghui; Scholten, Jan Christoph: Additional porewater, bottom water and solid phase geochemical and Ni isotope data for sediment cores collected during AL543 [dataset bundled publication]. PANGAEA, https://doi.pangaea.de/10.1594/PANGAEA.974022

Declaration of competing interest

The authors declare that they have no known competing financial interests or personal relationships that could have appeared to influence the work reported in this paper.

Acknowledgments

This research was supported by SNSF grant 200021_184873/1 to DV and the DFG Emmy Noether Group ICONOX to FS. JD is supported by The Fundamental Research Funds for the Central Universities, Peking University. We would like to thank the crew of RV Alkor as well as our colleagues Corey Archer, Anna Plass, Paul Vosteen, Regina Surberg,

Andrea Bodenbinder, Bettina Domeyer, Anna-Kathrin Retschko and Anke Bleyer for their support during research at sea and during the post-cruise work.

Appendix A. Supplementary material

This paper is associated with a single Supplementary Materials file, which contains one supplementary Figure (S1) and five supplementary Tables (S1-S5) as follows: Fig. S1 showing bulk and authigenic Ni/TOC for all the Kiel Bight sediment cores studied; Table S1 containing site locations as well as pore water chemical compounds, Mn, Fe and Ni concentrations and δ^{60}Ni as a function of depth below the sediment water interface; Table S2 containing data for Kiel Bight bottom waters from the benthic trace profiler, including H_2S, PO_4^{3-}, Si, Mn, Fe, Ni concentrations and Ni isotope compositions; Table S3 containing Ni and P concentrations in water column particulate material from the benthic trace profiler; Table S4 containing solid phase (sediment) chemistry and Ni isotope compositions as a function of depth below the sediment–-water interface; Table S5 containing mass accumulation rates for all Kiel Bight cores studied.

Supplementary material to this article can be found online at https://doi.org/10.1016/j.gca.2025.01.016.

References

Appleby, P.G., Oldfieldz, F., 1983. The assessment of ^{210}Pb data from sites with varying sediment accumulation rates. Hydrobiologia 103, 29–35.

Archer, C., Vance, D., Milne, A., Lohan, M.C., 2020. The oceanic biogeochemistry of nickel and its isotopes: new data from the South Atlantic and the Southern Ocean biogeochemical divide. Earth Planet. Sci. Lett. 535, 116118.

Atkins, A.L., Shaw, S., Peacock, C.L., 2016. Release of Ni from birnessite during transformation of birnessite to todorokite: implications for Ni cycling in marine sediments. Geochim. Cosmochim. Acta 189, 158–183.

Berelson, W.M., McManus, J., Coale, K.H., Johnson, K.S., Kilgore, T., Burdige, D.J., Pilskaln, C., 1996. Biogenic matter diagenesis on the sea floor: a comparison between two continental margin transects. J. Mar. Res. 54 (4).

Bian, X., Yang, S.C., Raad, R.J., Lunstrum, A.M., Dong, S., Meng, H., Kemnitz, N., Rollins, N.E., Cetiner, J.E.P., Pavia, F.J., Hammond, D.E., Adkins, J.F., Berelson, W. M., John, S.G., 2024a. A benthic source of isotopically heavy Ni from continental margins and implications for global ocean Ni isotope mass balance. Earth Planet. Sci. Lett. 645, 118951.

Bian, X., Yang, S.C., Raad, R.J., Odendahl, C.E., Lanning, N.T., Sieber, M., Huang, K.-F., Fitzsimmons, J.N., Conway, T.M., John, S.G., 2024b. Distribution and cycling of nickel and nickel isotopes in the Pacific Ocean. Geophys. Res. Lett. 51, 2024GL1111115.

Böning, P., Brumsack, H.J., Böttcher, M.E., Schnetger, B., Kriete, C., Kallmeyer, J., Borchers, S.L., 2004. Geochemistry of Peruvian near-surface sediments. Geochim. Cosmochim. Acta 68 (21), 4429–4451.

Böning, P., Cuypers, S., Grunwald, M., Schnetger, B., Brumsack, H.J., 2005. Geochemical characteristics of Chilean upwelling sediments at~ 36° S. Mar. Geol. 220 (1–4), 1–21.

Böning, P., Brumsack, H.J., Schnetger, B., Grunwald, M., 2009. Trace element signatures of Chilean upwelling sediments at~ 36 S. Mar. Geol. 259 (1–4), 112–121.

Böning, P., Shaw, T., Pahnke, K., Brumsack, H.J., 2015. Nickel as indicator of fresh organic matter in upwelling sediments. Geochim. Cosmochim. Acta 162, 99–108.

Boudreau, B.P., 1996. The diffusive tortuosity of fine-grained unlithified sediments. Geochim. Cosmochim. Acta 60 (16), 3139–3142.

Bruggmann, S., McManus, J., Archer, C., Vance, D., Severmann, S., 2024. Nickel's behaviour in marine sediments under aerobic to anaerobic diagenetic conditions. Chem, Geol.

Bruland, K.W., 1980. Oceanographic distributions of cadmium, zinc, nickel, and copper in the North Pacific. Earth Planet. Sci. Lett. 47 (2), 176–198.

Brumsack, H.J., 1989. Geochemistry of recent TOC-rich sediments from the Gulf of California and the Black Sea. Geol. Rundsch. 78, 851–882.

Cameron, V., Vance, D., 2014. Heavy nickel isotope compositions in rivers and the oceans. Geochim. Cosmochim. Acta 128, 195–211.

Chen, X., Ling, H.F., Vance, D., Shields-Zhou, G.A., Zhu, M., Poulton, S.W., Och, L.M., Jiang, S., Li, D., Cremoneses, L., Archer, C., 2015. Rise to modern levels of ocean oxygenation coincided with the Cambrian radiation of animals. Nat. Commun. 6 (1), 7142.

Ciscato, E.R., Bontognali, T.R., Vance, D., 2018. Nickel and its isotopes in organic-rich sediments: implications for oceanic budgets and a potential record of ancient seawater. Earth Planet. Sci. Lett. 494, 239–250.

Cutter, G., Andersson, P., Codispoti, L., Croot, P., Francois, R., Lohan, M., Obata, H., Rutgers, M., 2014. Sampling and Sample-handling Protocols for GEOTRACES Cruises, Version 2.0, December 2014.

Dahl, T.W., Anbar, A.D., Gordon, G.W., Rosing, M.T., Frei, R., Canfield, D.E., 2010. The behavior of molybdenum and its isotopes across the chemocline and in the sediments of sulfidic Lake Cadagno. Switzerland. Geochim. Cosmochim. Acta 74 (1), 144–163.

Dale, A.W., Bertics, V.J., Treude, T., Sommer, S., Wallmann, K., 2013. Modeling benthic–pelagic nutrient exchange processes and porewater distributions in a seasonally hypoxic sediment: evidence for massive phosphate release by Beggiatoa? Biogeosciences 10 (2), 629–651.

Dale, A.W., Sommer, S., Lomnitz, U., Montes, I., Treude, T., Liebetrau, V., Hensen, C., Dengler, M., Stolpovsky, K., Bryant, L.D., Wallmann, K., 2015. Organic carbon production, mineralisation and preservation on the Peruvian margin. Biogeosci. 12 (5), 1537–1559.

Dargahi, B., Kolluru, V., Cvetkovic, V., 2017. Multi-layered stratification in the Baltic Sea: insight from a modeling study with reference to environmental conditions. J. Mar. Sci. Eng. 5 (1), 2.

Fleischmann, S., Du, J., Chatterjee, A., McManus, J., Iyer, S.D., Amonkar, A., Vance, D., 2023. The nickel output to abyssal pelagic manganese oxides: a balanced elemental and isotope budget for the oceans. Earth Planet. Sci. Lett. 619, 118301.

Fujii, T., Moynier, F., Blichert-Toft, J., Albarède, F., 2014. Density functional theory estimation of isotope fractionation of Fe, Ni, Cu, and Zn among species relevant to geochemical and biological environments. Geochim. Cosmochim. Acta 140, 553–576.

Gall, L., Williams, H.M., Siebert, C., Halliday, A.N., Herrington, R.J., Hein, J.R., 2013. Nickel isotopic compositions of ferromanganese crusts and the constancy of deep ocean inputs and continental weathering effects over the Cenozoic. Earth Planet. Sci. Lett. 375, 148–155.

Gäng, F., Böning, P., Brüchert, V., Lahajnar, N., Pahnke, K., 2023. Critical assessment of U, Ba and Ni as redox and productivity proxies in organic-rich sediments underneath dynamic, highly productive waters. Geochim. Cosmochim. Acta 348, 206–220.

Goldberg, E.D., 1954. Marine geochemistry 1. Chemical scavengers of the sea. J. Geol. 62 (3), 249–265.

Graf, G., Schulz, R., Peinert, R., Meyer-Reil, L.A., 1983. Benthic response to sedimentation events during autumn to spring at a shallow-water station in the Western Kiel Bight: I. Analysis of processes on a community level. Mar. Biol. 77, 235–246.

Grasshoff, K., Kremling, K., Ehrhardt, M., 1999. Methods of seawater analysis. Wiley-VCH Verlag.

Gueguen, B., Rouxel, O., 2021. The Nickel isotope composition of the authigenic sink and the diagenetic flux in modern oceans. Chem. Geol. 563, 120050.

Gueguen, B., Rouxel, O., Rouget, M.L., Bollinger, C., Ponzevera, E., Germain, Y., Fouquet, Y., 2016. Comparative geochemistry of four ferromanganese crusts from the Pacific Ocean and significance for the use of Ni isotopes as paleoceanographic tracers. Geochim. Cosmochim. Acta 189, 214–235.

Gueguen, B., Rouxel, O., Fouquet, Y., 2021. Nickel isotopes and rare earth elements systematics in marine hydrogenetic and hydrothermal ferromanganese deposits. Chem. Geol. 560, 119999.

Hansen, H.P., Giesenhagen, H.C., Behrends, G., 1999. Seasonal and long-term control of bottom-water oxygen deficiency in a stratified shallow-water coastal system. ICES J. Mar. Sci. 56, 65–71.

He, Z., Clarkson, M.O., Andersen, M.B., Archer, C., Sweere, T.C., Kraal, P., Guthauser, A., Huang, F., Vance, D., 2021. Temporally and spatially dynamic redox conditions on an upwelling margin: the impact on coupled sedimentary Mo and U isotope systematics, and implications for the Mo-U paleoredox proxy. Geochim. Cosmochim. Acta 309, 251–271.

He, Z., Archer, C., Yang, S., Vance, D., 2023. Sedimentary cycling of zinc and nickel and their isotopes on an upwelling margin: implications for oceanic budgets and paleoenvironment proxies. Geochim. Cosmochim. Acta 343, 84–97.

Helz, G.R., Vorlicek, T.P., Kahn, M.D., 2004. Molybdenum scavenging by iron monosulfide. Environ. Sci. Tech. 38 (16), 4263–4268.

Lemaitre, N., Du, J., de Souza, G.F., Archer, C., Vance, D., 2022. The essential bioactive role of nickel in the oceans: evidence from nickel isotopes. Earth Planet. Sci. Lett. 584, 117513.

Lennartz, S.T., Lehmann, A., Herrford, J., Malien, F., Hansen, H.P., Biester, H., Bange, H. W., 2014. Long-term trends at the Boknis Eck time series station (Baltic Sea), 1957–2013: does climate change counteract the decline in eutrophication? Biogeosciences 11 (22), 6323–6339.

Li, Y.-H., Gregory, S., 1974. Diffusion of ions in sea water and in deep-sea sediments. Geochim. Cosmochim. Acta 38 (5), 703–714.

Little, S.H., Vance, D., Lyons, T.W., McManus, J., 2015. Controls on trace metal authigenic enrichment in reducing sediments: insights from modern oxygen-deficient settings. Am. J. Sci. 315 (2), 77–119.

Little, S.H., Archer, C., McManus, J., Najorka, J., Wegorzewski, A.V., Vance, D., 2020. Towards balancing the oceanic Ni budget. Earth Planet. Sci. Lett. 547, 116461.

Mackey, D.J., O'Sullivan, J.E., Watson, R.J., Dal Pont, G., 2002. Trace metals in the Western Pacific: temporal and spatial variability in the concentrations of Cd, Cu, Mn and Ni. Deep Sea Res. Part I 49 (12), 2241–2259.

Manheim, F. T., Lane-Bostwick, C. M., 1989. Chemical composition of ferromanganese crusts in the world ocean: a review and comprehensive database. Open-File Report 89-020, U.S. Geological Survey, Woods Hole, MA.

Perner, M., Wallmann, K., Adam-Beyer, N., Hepach, H., Laufer-Meiser, K., Böhnke, S., Diercks, I., Bange, H.W., Indenbirken, D., Nikeleit, V., Bryce, C., Kappler, A., Engel, A., Scholz, F., 2022. Environmental changes affect the microbial release of hydrogen sulfide and methane from sediments at Boknis Eck (SW Baltic Sea). Front. Microbiol. 13, 1096062.

Plass, A., Dale, A.W., Scholz, F., 2021. Sedimentary cycling and benthic fluxes of manganese, cobalt, nickel, copper, zinc and cadmium in the Peruvian oxygen minimum zone. Mar. Chem. 233, 103982.

Plass, A., Retschko, A.K., Türk, M., Fischer, T., Scholz, F., 2022. A novel device for trace metal-clean sampling of bottom water and suspended particles at the ocean's lower boundary: the Benthic Trace Profiler. Limnol. Oceanogr. Methods 20 (2), 102–114.
Ragsdale, S.W., 2009. Nickel-based enzyme systems. J. Biol. Chem. 284 (28), 18571–18575.
Reinhard, C.T., Planavsky, N.J., Robbins, L.J., Partin, C.A., Gill, B.C., Lalonde, S.V., Bekker, A., Konhauser, K.O., Lyons, T.W., 2013. Proterozoic ocean redox and biogeochemical stasis. PNAS 110 (14), 5357–5362.
Revels, B.N., Rickli, J., Moura, C.A., Vance, D., 2021. Nickel and its isotopes in the Amazon Basin: the impact of the weathering regime and delivery to the oceans. Geochim. Cosmochim. Acta 293, 344–364.
Sanchez-Cabeza, J.A., Ruiz-Fernández, A.C., 2012. ^{210}Pb sediment radiochronology: an integrated formulation and classification of dating models. Geochim. Cosmochim. Acta 82, 183–200.
Scholz, F., Cheng, J., Zhang, Z., Vosteen, P., Siebert, C., Frank, M., 2023. Benthic-pelagic coupling and isotopic fractionation of barium in Kiel Bight. SW Baltic Sea. Front. Mar. Sci. 10, 1101095.
Sclater, F.R., Boyle, E., Edmond, J.M., 1976. On the marine geochemistry of nickel. Earth Planet. Sci. Lett. 31 (1), 119–128.
Scott, C., Lyons, T.W., Bekker, A., Shen, Y.A., Poulton, S.W., Chu, X.L., Anbar, A.D., 2008. Tracing the stepwise oxygenation of the Proterozoic ocean. Nature 452 (7186), 456–459.
Seibold, E., Exon, N., Hartmann, M., Kögler, F.-C., Krumm, H., Lutze, G. F., Newton, R. S., Werner, F., 1971. Marine Geology of Kiel Bay. In: Sedimentology of Parts of Central Europe, Guidebook VIII (Heidelberg, Germany: International Sedimentology Congress), 209-235.
Smetacek, V., 1981. The annual cycle of protozooplankton in the Kiel Bight. Mar. Biol. 63 (1), 1–11.
Sorensen, J.V., Gueguen, B., Stewart, B.D., Peña, J., Rouxel, O., Toner, B.M., 2020. Large nickel isotope fractionation caused by surface complexation reactions with hexagonal birnessite. Chem. Geol. 537, 119481.
Stookey, L.L., 1970. Ferrozine – a new spectrophotometric reagent for iron. Anal. Chem. 42 (7), 779–781.
Sun, M., Archer, C., Vance, D., 2021. New methods for the chemical isolation and stable isotope measurement of multiple transition metals, with application to the earth sciences. Geostand. Geoanal. Res. 45 (4), 643–658.
Tegler, A., Horner, T.J., Galy, V., Bent, S.M., Wang, Y., Kim, H.H., Öykü, Z.M., Nielsen, S. G., 2024. Distribution and drivers of organic carbon sedimentation along the continental margins. AGU Adv. 5, e2023AV001000.
Twining, B.S., Baines, S.B., 2013. The trace metal composition of marine phytoplankton. Annu. Rev. Mar. Science 5, 191–215.
Twining, B.S., Baines, S.B., Fisher, N.S., 2004. Element stoichiometries of individual plankton cells collected during the Southern Ocean Iron Experiment (SOFeX). Limnol. Oceanogr. 49 (6), 2115–2128.
Twining, B.S., Nunez-Milland, D., Vogt, S., Johnson, R.S., Sedwick, P.N., 2010. Variations in Synechococcus cell quotas of phosphorus, sulfur, manganese, iron, nickel, and zinc within mesoscale eddies in the Sargasso Sea. Limnol. Oceanogr. 55 (2), 492–506.
Twining, B.S., Baines, S.B., Bozard, J.B., Vogt, S., Walker, E.A., Nelson, D.M., 2011. Metal quotas of plankton in the equatorial Pacific Ocean. Deep Sea Res. Part II 58 (3–4), 325–341.
Uramoto, G.I., Morono, Y., Tomioka, N., Wakaki, S., Nakada, R., Wagai, R., Uesugi, K., Takeuchi, A., Hoshino, M., Suzuki, Y., Shiraishi, F., Mitsunobu, S., Suga, H., Takeichi, Y., Takahashi, Y., Inagaki, F., 2019. Significant contribution of subseafloor microparticles to the global manganese budget. Nat. Commun. 10 (1), 1–10.
van der Weijden, C.H., Reichart, G.J., van Os, B.J., 2006. Sedimentary trace element records over the last 200 kyr from within and below the northern Arabian Sea oxygen minimum zone. Mar. Geol. 231 (1–4), 69–88.
Vance, D., Little, S.H., Archer, C., Cameron, V., Andersen, M.B., Rijkenberg, M.J., Lyons, T.W., 2016. The oceanic budgets of nickel and zinc isotopes: the importance of sulfidic environments as illustrated by the Black Sea. Philos. Trans. R. Soc. London, Ser. A 374 (2081), 20150294.
Wang, S.J., Rudnick, R.L., Gaschnig, R.M., Wang, H., Wasylenki, L.E., 2019. Methanogenesis sustained by sulfide weathering during the Great Oxidation Event. Nat. Geosci. 12, 296–300.